⌘ *Author's Choice*

THE JOURNAL OF BIOLOGICAL CHEMISTRY VOL. 287, NO. 28, pp. 23381–23396, July 6, 2012

Structural and Mechanistic Studies of Pesticin, a Bacterial Homolog of Phage Lysozymes*[S]

Received for publication, March 18, 2012, and in revised form, April 26, 2012 Published, JBC Papers in Press, May 16, 2012, DOI 10.1074/jbc.M112.362913

Silke I. Patzer[1], **Reinhard Albrecht, Volkmar Braun, and Kornelius Zeth**[2]

From the Department of Protein Evolution, Max Planck Institute for Developmental Biology, Spemannstrasse 35, 72076 Tübingen, Germany

Background: Pesticin is a protein toxin that is formed by *Yersinia pestis* to kill related strains.
Results: The crystal structure and functional analyses revealed a receptor binding, a translocation, and an activity domain.
Conclusion: Folding of the activity domain is very similar to folding of phage T4 lysozyme.
Significance: This is the first case that an activity domain is derived from a known enzyme.

Yersinia pestis **produces and secretes a toxin named pesticin that kills related bacteria of the same niche. Uptake of the bacteriocin is required for activity in the periplasm leading to hydrolysis of peptidoglycan. To understand the uptake mechanism and to investigate the function of pesticin, we combined crystal structures of the wild type enzyme, active site mutants, and a chimera protein with *in vivo* and *in vitro* activity assays. Wild type pesticin comprises an elongated N-terminal translocation domain, the intermediate receptor binding domain, and a C-terminal activity domain with structural analogy to lysozyme homologs. The full-length protein is toxic to bacteria when taken up to the target site via the outer or the inner membrane. Uptake studies of deletion mutants in the translocation domain demonstrate their critical size for import. To further test the plasticity of pesticin during uptake into bacterial cells, the activity domain was replaced by T4 lysozyme. Surprisingly, this replacement resulted in an active chimera protein that is not inhibited by the immunity protein Pim. Activity of pesticin and the chimera protein was blocked through introduction of disulfide bonds, which suggests unfolding as the prerequisite to gain access to the periplasm. Pesticin, a muramidase, was characterized by active site mutations demonstrating a similar but not identical residue pattern in comparison with T4 lysozyme.**

Bacteriocins are proteinaceous toxins produced by many Gram-negative bacteria to inhibit the growth of closely related bacterial strains. Pesticin (Pst)[3] from *Yersinia pestis* is a toxin that kills *Y. pestis, Yersinia enterocolitica,* and certain *Escherichia coli* strains (1). It belongs to the large group of bacteriocins from Gram-negative bacteria of which the colicins derived from *E. coli* strains are the largest and best studied class (1). Nearly half of the natural *E. coli* isolates produce colicins (1). Although *Y. pestis* includes only one plasmid-encoded toxin, *E. coli* can encode a variety of up to 21 colicins (1). Bacteria within natural populations losing the bacteriocin-coding plasmid may be killed by the surrounding bacteria that produce bacteriocins. Bacteriocin-producing cells are protected from suicide after re-uptake of toxins by expression of small immunity proteins.

The large class of colicins displays a variety of enzymatic functions among which are nucleases for the degradation of DNA, rRNA, or tRNA (1). A second class of colicins forms pores in the inner membrane that dissipate the electrochemical potential (1). Currently, only two bacteriocins are known to develop activity in the periplasm. Colicin M inhibits peptidoglycan (PG) biosynthesis (2), whereas pesticin is a muramidase that degrades PG (3, 4). The genetic organization and the principal structural architecture of Pst resemble colicins. The *pst* operon encodes Pst and the Pim protein, an antagonist to pesticin also known as the immunity protein that confers pesticin resistance to Pst-producing cells. Pim resides in the periplasm where the PG substrate of Pst is located (5).

Colicins are the only proteins actively imported by *E. coli* cells, which make them particularly attractive for studies of bacterial protein import. Colicin activity requires at least three steps as follows: 1) binding on the cell surface via receptor recognition; 2) energy-dependent uptake into the compartment of activity, and 3) destruction of the cellular target. Colicins denoted as group A colicins are imported across the outer membrane by the Tol system, whereas group B colicins use the Ton system for import. Colicins are typically composed of three domains as follows: the N-terminal translocation domain (T domain) comprising the TonB box segment that is important for binding to TonB and subsequent uptake across the outer membrane. Uptake requires energy that is generated by the protonmotive force of the cytoplasmic membrane. The energy-coupling machinery transforming electrochemical energy into the pulling force for colicin import consists of the TonB, ExbB, and ExbD proteins that are all anchored in the cytoplasmic

* This work was supported by the Max Planck Society and the Fonds der Chemischen Industrie (to V. B.).
⌘ *Author's Choice*—Final version full access.
[S] This article contains supplemental Figs. S1–S8 and additional references.
The atomic coordinates and structure factors (codes 4AQN, 4ARQ, 4ARM, 4ARL, 4ARP, and 4ARJ) have been deposited in the Protein Data Bank, Research Collaboratory for Structural Bioinformatics, Rutgers University, New Brunswick, NJ (http://www.rcsb.org/).
[1] To whom correspondence may be addressed. Tel.: 49-7071-601345; Fax: 49-7071-601349; E-mail: silke.patzer@tuebingen.mpg.de.
[2] To whom correspondence may be addressed: ZMBP, University of Tübingen, Auf der Morgenstelle 1, 72076 Tübingen, Germany. E-mail: kornelius.zeth@googlemail.com.
[3] The abbreviations used are: Pst, pesticin; SeMet, selenomethionine; PDB, Protein Data Bank; HEWL, hen egg white lysozyme; PG, peptidoglycan; Ni-NTA, nickel-nitrilotriacetic acid; PEG, polyethylene glycol.

membrane (1). This complex recognizes via TonB N-terminal TonB box sequences of outer membrane receptor proteins and bacteriocins, which results in import of the receptor-bound ligands into the periplasm.

The central receptor binding domain (R domain) is essential for the intimate contact with the outer membrane protein receptor, and the C-terminal activity domain (A domain) includes the deathly activity. Crystal structures of colicin R domains bound to receptors have been solved for colicins E2 and E3 bound to the BtuB receptor (6, 7) and for colicin Ia bound to the Cir receptor (8). Binding of the E3 colicin to BtuB induces local unfolding in the R domain, which is believed to be transmitted to the T domain (6). The receptor-bound R domain of the Ia structure does not differ from the R domain in the structure of the isolated complete Ia. Structural changes in both receptors do not open the pore within the β-barrel. After the first intimate contact of colicins E2 and E3 with BtuB, the bacterial porin OmpF is recruited to form a ternary complex through which the colicins are imported (6, 8). In contrast, colicin Ia first binds to Cir and then to a second Cir for translocation across the outer membrane (9). Despite detailed structural and functional information, the translocation mechanism through receptors remains unknown.

FyuA is an energy-coupled receptor in the outer membrane of *Y. pestis* through which the iron siderophore yersiniabactin and Pst are taken up into the periplasm. Some *E. coli* strains also express FyuA and are killed by Pst (10). After binding to FyuA, Pst uptake proceeds by a direct contact of the FyuA TonB box with TonB with subsequent translocation into the periplasm. In the bacterial periplasm Pst hydrolyzes PG by cleaving the bond between the C1 of *N*-acetylmuramic acid and C4 of *N*-acetylglucosamine (lysozyme activity) (4). In the absence of an intact PG layer, the cytoplasmic membrane no longer withstands the cytoplasmic osmotic pressure, and cells undergo lysis. Pst slowly hydrolyzes PG, which results in the formation of osmotically stable spheroplast-like forms. The spheroplast-like structures are obtained in the absence of sucrose to adapt the external osmotic pressure to the internal osmotic pressure. Nevertheless, addition of Pst to exponentially growing cells results in immediate dose-dependent loss of the ability to form colonies (3).

Very little is known about the mechanisms by which bacteriocins are translocated across the outer membrane. In particular, the transient steps for successive structural unfolding during translocation lack experimental tracing. To extract geometrical parameters influential for bacteriocin uptake, we chose the PG-degrading enzyme Pst and extended our previous functional studies (4, 5) toward a mechanistic understanding. To this end, we determined crystal structures of pesticin, Pst mutants, and a pesticin-T4 lysozyme chimera, and these structural studies were supported by functional studies regarding Pst uptake and activity. Together, these experiments allowed us to dissect the role of the R, T, and A domains in uptake and unfolding during translocation. Moreover, by mutational analysis we tested putative active site residues that we found to be overlapping but not identical to related lysozyme proteins. Taken together, these studies provide a structural view of Pst and advance knowledge of the uptake and plasticity of this bacteriocin.

EXPERIMENTAL PROCEDURES

Recombinant DNA Techniques—Plasmids were manipulated according to the methods of Sambrook and Russell (11). Plasmids were isolated and purified on a silica matrix with PureYield columns (Promega, Mannheim, Germany). Oligonucleotides were synthesized by Eurofins MWG Operon (Ebersberg, Germany). PCRs were performed with a Mastercycler ep gradient S (Eppendorf, Hamburg, Germany) and the Phusion DNA polymerase (Finnzymes, Espoo, Finland). DNA sequencing was carried out with the BigDye terminator version 3.1 cycle sequencing kit (Applied Biosystems, Foster City, CA). Samples were run on a 3730xl DNA analyzer (Applied Biosystems), a service provided by the Max Planck Institute for Developmental Biology.

Construction of Plasmids and Strains—The *E. coli* strains and plasmids used in this work are given in Table 1. For construction of plasmids, overhanging DNA ends were made blunt prior to ligation. Vectors were dephosphorylated with calf intestine alkaline phosphatase (Fermentas, St. Leon-Rot, Germany), and PCR products were phosphorylated by T4 polynucleotide kinase (Fermentas). The ligation products were introduced into *E. coli* DH5α (Stratagene, Heidelberg, Germany). The construct sequences were confirmed by DNA sequencing.

Pst Constructs—The genes encoding Pst, Pst^{RT}, and Pst^{A} with a C-terminal His tag were cloned by PCR amplification from pUH64 (4) with the primer pairs TGTCAGATACAATGGTAGTGAATGGTTC and GTTTTAACAATCCACTATCGATATCTTTTTGCAC, TGTCAGATACAATGGTAGTGAATGGTTC and GAACAATATTTACCGAACGACGTAAAAATTCC, and TGGTAAATATTGTTGACCACGATATTTTCTC and GTTTTAACAATCCACTATCGATATCTTTTTGCAC and ligation into the NdeI/XhoI cut expression vector pET22b (Novagen, Darmstadt, Germany) resulting in plasmids pSP130/70, pSP130/64, and pSP130/66, respectively. Pst was fused to a signal sequence on pUH64 that was amplified by PCR with the primers TGTCAGATACAATGGTAGTGAATGGTTC and GTTTTAACAATCCACTATCGATATCTTTTTGCAC, ligated to a sequence encoding a C-terminal His tag, and cloned downstream of *malE*′ of pMA-RQ MalE′-Cma1–130 synthesized by Geneart (Regensburg, Germany) as described previously (12), replacing *cma1–130*. The resulting plasmid pSP130/151 encodes the signal sequence MalE(1–26) (Swissprot P0AEX9), Pst, and the C-terminal His tag LAHHHHHH under control of the *araBAD* promoter and contains *araC*. The plasmid encoding the activity domain Pst^{A} equipped with a signal sequence was cloned accordingly with the primers TGGTAAATATTGTTGACCACGATATTTTCTC and GTTTTAACAATCCACTATCGATATCTTTTTGCAC resulting in pSP130/152.

Pst-T4L Chimera Constructs—The gene encoding the T4 lysozyme derivative T4L (C221T and C264A) was amplified by PCR with the primers TGAATATATTTGAAATGTTACGTATAGATGAAGG and ATAGATTTTTATACGCGTCCCAAGTGCC from plasmid T4L, which was kindly provided by Joachim E. Schultz, University of Tübingen, Germany. The PCR

TABLE 1
***E. coli* strains and plasmids used in this work**

Strain, plasmid	Genotype or description	Ref. or source
***E. coli* strains**		
BL21(DE3)	*hsdS* ($r_B^- m_B^-$) *gal dcm ompT* λ(DE3), T7 RNA polymerase gene under control of the *lac*UV5 promoter	51
C41	Derivative of BL21 (DE3)	52
SIP1332	C41 pSP130/29	This study
SIP1453	As SIP1332 but *tonB*	This study
SIP1461	As SIP1332 but *fhuA*	This study
Plasmids		
pHM10	pACYC184 encoding FyuA	53
pSP130/29	pET25b encoding FyuA with His tag at N terminus of mature protein	This study
pSP130/33	pET22b encoding Pim-His_6	This study
pSP130/64	pET22b encoding Pst(1–167)-His_6 (Pst^{RT})	This study
pSP130/66	pET22b encoding Pst(164–357)-His_6 (Pst^{A})	This study
pSP130/70	pET22b encoding Pst(1–357)His_6 (Pst)	This study
pSP130/73	pET22b encoding Pst^{Q301A}-His_6	This study
pSP130/88	pET22b encoding Pst^{P187A}-His_6	This study
pSP130/92	pET22b encoding Pst^{T201A}-His_6	This study
pSP130/110	pET22b encoding Pst^{E178A}-His_6	This study
pSP130/467	pET22b encoding $Pst^{S89C/S285C}$-His_6	This study
pSP130/480	pET22b encoding Pst^{D338A}-His_6	This study
pSP130/486	pET22b encoding Pst^{D207A}-His_6	This study
pSP130/258	pET22b encoding $Pst^{\Delta 10-15}$-His_6	This study
pSP130/262	pET22b encoding $Pst^{\Delta 10-20}$-His_6	This study
pSP130/375	pET22b encoding T4L-His_6; T4L refers to LYS_BPT4 Swiss-Prot P00720 with replacement of the two intrinsic cysteine residues (C221T/C264A)	This study
pSP130/187	pET24d encoding Pst-T4L-His_6	This study
pSP130/432	pET24d encoding Pst-$T4L^{D294C/R321C}$-His_6	This study
pSP130/379	pET24d encoding Pst-$T4L^{I176C/R321C}$-His_6	This study
pSP130/441	pET24d encoding Pst-$T4L^{I176C/L331C}$-His_6	This study
pSP130/452	pET24d encoding Pst-$T4L^{S257C/Q289C}$-His_6	This study
pSP130/151	Encodes MalE (1–26)-Pst with a C-terminal His tag (MalE′-Pst) controlled by the *araBAD* promoter, *araC*, Amp^r	This study
pSP130/152	Encodes MalE (1–26)-Pst (164–357) with a C-terminal His tag (MalE′-Pst^{A}) under control of the *araBAD* promoter, *araC*, Amp^r	This study
pSP130/176	Encodes MalE′-Pst^{E178A} with a C-terminal His tag under control of the *araBAD* promoter, *araC*, Amp^r	This study
pSP130/178	Encodes MalE′-$Pst^{A\ (E178A)}$ with a C-terminal His tag under control of the *araBAD* promoter, *araC*, Amp^r	This study

product was cloned into the NdeI/XhoI cut expression vector pET22b yielding pSP130/375 and into pPstT7Lys (Trenzyme Biotechnology, Konstanz, Germany) replacing the T7 lysozyme gene yielding pSP130/187.

N-terminal Pst Deletion Constructs—The deletion encoding $Pst^{\Delta 10-15}$ was generated by PCR amplification of pSP130/70 with the primers ACCATTCACTACCATTGTATCTGACATAAAA and TTTCTCTTTTCCGGAAGTACATTAAGCAG and subsequent ligation, resulting in plasmid pSP130/258. For $Pst^{\Delta 10-20}$ plasmid pSP130/262 was generated accordingly with the primers ACCATTCACTACCATTGTATCTGACATAAAA and AGTACATTAAGCAGTTACAGACCAAATTTTG.

Active Site Mutants of Pst—Site-directed mutagenesis was performed by PCR with two complementary primers containing the mutation (primer sequences are available upon request) and treatment with DpnI (Fermentas) prior to transformation of DH5α (13).

FyuA Construct—fyuA, including the stop codon, was amplified by PCR from pHM10 and cloned into the NdeI/XhoI cut vector pET25b (Novagen). The sequence CATCATCACCATCATGCGGCCGCACTC encoding His_5-Ala-Ala-Ala-Leu was inserted between the sequence encoding the signal peptide and the sequence encoding mature FyuA, yielding plasmid pSP130/29.

Pim Construct—Plasmid pSP130/33 was constructed by amplification of *pim* from pUH64 by PCR with the primers TGATCTCAAAGTTATTTTGCTTGGCTCTC and AATGATAATATACAGTGCAACCAGGG and ligation of the product into the NdeI/XhoI cut vector pET22b.

Mutant Strains—The chromosomal *tonB* mutant SIP1453 was obtained by selecting for Cma-resistant colonies of SIP1332. Sequencing revealed a point mutation resulting in a TonB109Stop mutation. The chromosomal *fhuA* mutant SIP1461 was gained by selecting for bacteriophage T5-resistant colonies of SIP1332. Sequencing revealed a point mutation resulting in an FhuA253Stop mutation.

Protein Overproduction and Purification—Pst without His tag was purified using a modified version of a protocol described previously (4). Briefly, *E. coli* BL21 (DE3) RIL (Stratagene) was transformed by electroporation with plasmid pUH64 that encodes the pesticin gene *pst* and the pesticin immunity gene *pim* downstream of gene 10 promoter of bacteriophage T7. Cells were grown at 37 °C in Luria Bertani (LB) medium supplemented with ampicillin (100 μg/ml) and chloramphenicol (25 μg/ml). When the A_{600} value reached 0.8, isopropyl β-D-1-thiogalactopyranoside was added to a final concentration of 1 mM. After 4 h of cultivation, cells were harvested and resuspended in 50 mM sodium phosphate buffer, pH 8.1. Cells were disrupted with a French press, and solid $(NH_4)_2SO_4$ was added to the soluble fraction to 50% saturation at which pesticin precipitated. The precipitate was solubilized in 20 mM Tris-HCl, pH 8.4, and dialyzed against this buffer. The solution was loaded on a Mono Q column (GE Healthcare) equilibrated with the Tris-HCl buffer (see above), and Pst eluted by applying a NaCl gradient in Tris-HCl. Fractions containing pesticin were pooled, dialyzed against 10 mM HEPES, pH 7.5, 50 mM NaCl, 3 mM $MgCl_2$, and the protein was concentrated to 41 mg/ml. The SeMet derivative was obtained by the same method with the

exception that cells were grown in M9 salt minimal medium supplemented with the amino acids Leu, Ile, Phe, Thr, Lys, and Val (14).

His tag versions of Pst^{WT}, Pst^{E178A}, Pst^{P187A}, Pst^{T201A}, Pst^{D207A}, Pst^{Q301A}, Pst^{D338A}, $Pst^{S89C/S285C}$, Pst^{RT}, Pst^{A}, $Pst^{\Delta 10-15}$, and $Pst^{\Delta 10-20}$ were purified from transformants of *E. coli* BL21(DE3) harboring the recombinant plasmids pSP130/70, pSP130/110, pSP130/88, pSP130/92, pSP130/486, pSP130/73, pSP130/480, pSP130/467, pSP130/64, pSP130/66, pSP130/258, and pSP130/262, respectively, on Ni-NTA-agarose (Qiagen) according to the manufacturer's protocol, taking advantage of the C-terminal His tag on the proteins. *E. coli* BL21(DE3) was not killed by Pst because it does not express the receptor FyuA. For synthesis of Pst^{RT} and Pst^{A}, cells were grown at 28 °C, because under these conditions approximately half of the protein was found in the soluble fraction, whereas virtually all protein was found in inclusion bodies when grown at 37 °C. Pst and the other Pst derivatives did not form inclusion bodies in significant amounts, and cells were grown at 37 °C.

Because Pst-T4L in high amounts is toxic for *E. coli* strains due to the T4 lysozyme activity, T4L, Pst-T4L, and its derivatives Pst-$T4L^{D294C/R321C}$, Pst-$T4L^{I176C/R321C}$, Pst-$T4L^{I176C/L331C}$, and Pst-$T4L^{S257C/Q289C}$ were overexpressed from pSP130/375, pSP130/187, pSP130/432, pSP130/379, pSP130/441, and pSP130/452, respectively, in *E. coli* C41 that carries mutations in the *lacUV5* promoter controlling the T7 RNA polymerase, which results in reduced T7 RNA polymerase levels. The proteins were purified on Ni-NTA-agarose.

Crystallization of Pst and Pst Derivatives—Initial sitting-drop crystallization trials of Pst were performed with the Honeybee 961 robot (Genomic solutions) using 13 commercial high throughput screens on 3:1 Corning 3550 96-well plates. Drops mixed from 0.4 μl of protein solution and 0.4 μl of reservoir solution were equilibrated against 75 μl of precipitant solution at 20 °C. Crystals of different shape appeared under a variety of conditions that were further reproduced under hanging-drop conditions. Needle-shaped crystals suitable for the x-ray data collection were obtained with a solution containing 18% PEG 8000, 0.2 M $MgCl_2$, and 0.1 M HEPES, pH 7.5. The Pst-SeMet construct was crystallized under the same conditions as Pst without the His tag. Pst^{T201A} and Pst^{E178A} were crystallized in a hanging-drop setup by mixing 1 μl of protein solution and 1 μl of ground solution, which contained 20% PEG 3350 and 0.2 M $NaNO_3$. Pst-T4L was crystallized in a hanging-drop setup by mixing 1.2 μl of protein solution and 0.8 μl of ground solution, which contained 20% PEG 3350 and 0.15 M K_2SO_4. For crystallization of Pst^{D207A}, the reservoir solution contained 20% PEG 3350 and 0.2 M NaI.

Structural Solution of SeMet-Pst, Pst, and Pst Mutants—The structure of Pst was solved by single anomalous diffraction methods using a SeMet-labeled Pst protein crystal. Protein crystals were flash-frozen in the presence of 15% glycerol for Pst, Pst^{T201A}, and Pst-T4L, 17% glycerol for Pst^{E178A}, and 20% PEG 400 for Pst^{D207A} added to the solution of crystallization conditions mentioned above. All x-ray crystallographic data were collected at beamline PX10 at the Swiss Light Source (SLS, Villigen, Switzerland). The crystals were kept at 100 K during data collection, and a 360° dataset was collected. Data were processed with the XDS/XSCALE (15) program package, and the structure was solved using the SHARP/autoSHARP program package (16, 17). Initial model building was performed in Arp/Warp and Buccaneer (18, 19). Subsequent improvement of models was achieved using the PHENIX program package in combination with Coot for the construction of the models (20, 21). The structure was analyzed using PROCHECK (22), and the figures were prepared using the PyMOL program package.

CD Spectroscopy—CD measurements were performed on a JASCO J-810 spectropolarimeter (Jasco, Gross-Umstadt, Germany) equipped with a thermoelectric temperature controller. All spectra were recorded with a 1-mm quartz cuvette at 190–250 nm using a bandwidth of 1 nm, a scanning speed of 100 nm min^{-1}, a data pitch of 0.2 nm, a response time of 1 s, and an accumulation of at least five spectra for averaging. Thermal denaturation was monitored at 222 nm between 10 and 90 °C with a temperature ramp of 1 °C min^{-1} and a data pitch of 0.5 °C. For data processing, subtracting the buffer base line, calculation of the melting temperature, and prediction of secondary structure, the Spectra Manager 2 software was used. Measurements were performed in 25 mM NaCl and 25 mM Tris-HCl, pH 7.5.

In Vivo Pesticin Activity Tests (Plaque Assay)—In vivo activity was tested using the sensitivity of an *E. coli* strain harboring a *fyuA* plasmid. LB plates (10 g of bacto tryptone, 5 g of yeast extract, 5 g of NaCl, 15 g of agar per liter) were overlaid with 3 ml of top agar seeded with 10^9 cells of the strain to be tested. 6 μl of 10-fold dilutions of pesticin solutions were spotted onto these plates. Following incubation overnight at 37 °C, the diameter of the lysis zones was measured. Cystine bridges were reduced by addition of 10 mM DTT. Cysteines were oxidized by 0.2 mM Cu^{2+} in complex with 1,10-phenanthroline.

In Vitro Lysozyme Assay—The sample was incubated in 50 mM NaCl and 50 mM Tris-HCl, pH 7.5, with fluorescein-labeled cell walls of *Micrococcus lysodeikticus* (Invitrogen) at 37 °C. Hydrolysis of the cell walls relieves fluorescence quenching, yielding a strong increase in fluorescence, which was measured with an excitation wavelength of 485 nm and an emission wavelength of 530 nm. The background fluorescence without sample was subtracted from each value.

Activity Assay for Secreted Pst—Cells synthesizing Pst and Pst^{A} fused to the MalE signal sequence were grown in LB medium containing ampicillin at 30 and 37 °C, respectively. It was not possible to grow *E. coli* containing pSP130/151 (encoding MalE′-Pst) at 37 °C even in the presence of glucose, because cells lysed. Because Pst is less toxic for *E. coli* cells at lower temperatures, this problem could be overcome by growth at 30 °C. In the exponential growth phase, arabinose was added to the final concentrations indicated. Cell growth and lysis were monitored by measuring the absorbance at 578 nm.

RESULTS

Crystallization and Structural Analysis of Pst, Pst Mutants, and Pesticin-T4 Lysozyme (Pst-T4L) Chimera—Pesticin was overproduced in *E. coli* cells harboring the plasmid encoding the wild type enzyme that was purified by previously established methods (4). The highly expressed protein devoid of any purification tag was purified by conventional methods to finally

achieve electrophoretic homogeneity (supplemental Fig. S1*A*). Crystals of the wild type protein were obtained that diffracted to a resolution of 1.98 Å (Table 2). The structure of Pst was solved by the single anomalous diffraction method using a single selenomethionine-labeled protein crystal. Additional Pst constructs (mutants and chimera) with C-terminal His tags were purified by Ni-NTA chromatography and subjected to crystallization. All structures were solved by molecular replacement using wild type Pst or the structure of T4L as search models. In total, we determined six crystal structures as follows: wild type Pst, a Pst cysteine double mutant ($Pst^{S89C/S285C}$), a Pst (residues 1–164)-T4L chimera (Pst-T4L), and three Pst active site mutants, Pst^{E178A}, Pst^{T201A}, and Pst^{D207A}. A summary of all refined structures, crystallization conditions, and data collection statistics is given in Table 2.

Pesticin, Three Domain Organization, and a Novel Phage Lysozyme Homolog—All bacteriocins consist of three domains as follows: the translocation domain, the receptor binding domain, and the activity domain. Accordingly, Pst includes a small and partially unfolded random coil translocation domain (residues 1 to ~40; Pst^{T}) with the eight N-terminal residues composing the TonB box element not visible in the electron density map (Fig. 1*A*). The elongated T domain with a molecular interface of 875 $Å^2$ to the R domain and high B-factors is rich in glycines (4), prolines (3), and serines (7), two of which (Ser-19 and Ser-21) are important for the alignment to the R domain surface. The FyuA receptor binding domain includes residues 41–166 (Pst^{R}) and is formed by a mixed α/β-fold. The β-sheet of seven anti-parallel β-strands ($\beta1$–$\beta7$) together with three helices displays the topology of $\beta1/\beta2/\beta3/\beta4/\beta5/\alpha1/\alpha2/\beta6/\beta7/\alpha3$ (Fig. 1*A*). β-Strands 1, 2, and 6, 7 are aligned almost parallel, and strands 3–5 are bent in a different angle (Fig. 1*A* for a topology scheme). This R domain does not display structural homology to any known domain of the PDB database and represents a novel fold (23). Notably, neither Pst^{T} nor Pst^{R} shows significant sequence homologies to the sequences in the Protein Data Bank. Therefore, the fold appears to have specifically adapted to bind to and to be taken up by the FyuA receptor.

The R and A domains are interconnected and stabilized relative to each other by 10 H-bonds forming a small interface of 530 $Å^2$ (see Fig. 1*A* for details). The activity domain includes residues 167–357 (Pst^{A}) and is an almost entirely α-helical domain ($\alpha4$–$\alpha11$) with three small β-strands ($\beta8$–$\beta10$) important for maintaining the active site architecture (Fig. 2). B-Factors of the active site vicinity are particularly low. The entire domain can be subdivided into two largely separated domains D1 (Pst^{AD1}; residues 167–266) and D2 (Pst^{AD2}; residues 267–357) interconnected by the long α-helical segment $\alpha7$ forming the active site cleft for substrate binding (Figs. 1*A* and 2*A*). This cleft has an approximate diameter of 1 nm and is sufficiently large to accommodate the PG substrate. Both areas facing the entry of this cleft show a strong positive charge profile with conserved arginine residues for substrate binding (Fig. 1, *B* and *C*). Although the T and R domains are unique in sequence, there are homologous sequences to Pst^{A} among the Pst-like proteins that after alignment indicate a particularly strong conservation of the active site residues Glu-178, Asp-207, and Thr-201 (see below) and more distant residues Gln-301, Arg-339, Arg-340, and Lys-341 (Fig. 1*C* and supplemental Fig. S6*B*). Moreover, additional residues in the backbone core of the lysozyme-like fold are conserved, some of which surround the active site and others extend from there to presumably stabilize this fold.

Pesticin, New Member of the Small Galaxy of Lysozyme Folds—The activity domain structure of Pst is unique and resembles the fold of a protein class of similar fold but of a biologically unrelated species. Similar sequences are classified into five large groups of T4-like lysozyme homologs as follows: 1) phage-related lysozymes, 2) a group of VgrG proteins comprising lysozyme domains, and 3) three smaller subclusters with pesticin as one representative (supplemental Fig. S2). Few structures of the clustering sequences have been solved, including the unrelated hen egg white lysozyme (HEWL), phage T4 lysozyme, the phage 21 endolysin domain, and a lysozyme-like fold as part of the gp5 protein (24). gp5 is part of the needle-like supramolecular punctuation structure of phage T4. Although all of these enzymes cleave PG, their individual fold may be quite diverse (Fig. 2). In comparison, Pst contains the largest domain with additional secondary structural elements not present in the related structures, in particular two helices located in the A_{D1} domain (Fig. 2*A*). The smallest microbial lysozyme is the p21 endolysin containing only three anti-parallel β-strands of the Pst^{AD1} domain and the A_{D2} domain. The Pst^{AD1}-like domains in T4 lysozyme and gp5 are essentially identical as they both derive from the same phage but serve different biological functions (Fig. 2, *B* and *D*). Although the three phage structures and the Pst largely coincide in the connection between A_{D1} and A_{D2} and their common four helix fold forming Pst^{AD2}, HEWL contains an entirely different fold of A_{D1} and A_{D2}. Here, both domains include a different number of secondary structural elements, a strongly shortened connecting helix, whereas almost the entire four helix bundle of A_{D2} is missing (Fig. 2*E*). Notably, all structures compared in Fig. 2 contain the unique fingerprint of the three β-sheets located in A_{D1}. In T4 lysozyme and HEWL, these sheets contain the most important residues for activity (25, 26). As T4 lysozyme, Pst hydrolyzes PG by cleaving the glycosidic bond between C1 of *N*-acetylmuramic acid and C4 of *N*-acetylglucosamine (muramidase activity) (4). The fold of the active centers of both enzymes is similar, but the residues of T4 lysozyme involved in binding and hydrolysis of the substrate differ in part (see below).

Binding and Translocation Studies of Pst, Importance of the R and T Domain—Pesticin is translocated across the outer membrane through the FyuA receptor that is coupled to the energy-delivering machinery of the cytoplasmic membrane formed by the proteins TonB, ExbB, and ExbD. Residues 3–7 of Pst represent the conserved TonB box motif (DTMVV) by which pesticin most likely interacts with TonB, as has been previously shown for colicins B (27), D (28), M (5), and Ia (8). It is unknown why most group B colicins in addition to their receptors need to interact with TonB. Translocation domains in bacteriocin structures often include an approximate length of ~40 N-terminal residues formed as random coil arrangement attached to the R domain. Examples are pesticin, colicin M (29), or colicin B (30), which show such elongated elements (Fig. 3, *A* and *B*).

TABLE 2
Data collection and refinement statistics

	Pst^{WT}	$Pst^{S89C/S285C}$	Pst^{T201A}	Pst^{D207A}	Pst^{E178A}	Pst-T4L
Data collection[a]						
Space group	$P2_1$	$P2_1$	$P2_1$	$P22_12_1$	$P2_12_12_1$	C2
Cell dimensions						
a, *b*, *c*	36.55, 86.78, 122.27 Å	35.96, 86.12, 122.02 Å	65.53, 43.21, 133.20 Å	35.32, 92.62, 225.92 Å	44.64, 127.83, 158.36 Å	194.87, 51.5, 107.92 Å
α, β, γ	90, 96.14, 90°	90, 97.48, 90°	90, 99.37, 90°	90°	90°	90, 91.01, 90°
Resolution	30 to 1.98 Å (2.02 to 1.98 Å)	36 to 2.6 Å (2.66 to 2.6 Å)	44 to 2.0 Å (2.03 to 2.0 Å)	58 to 2 Å (2.05 to 2.0 Å)	79 to 2.3 Å (2.34 to 2.3 Å)	73 to 2.6 Å (2.66 to 2.6 Å)
R_{sym} or R_{merge}	0.1 (0.65)	0.04 (0.21)	0.09 (0.42)	0.06 (0.48)	0.13 (0.81)	0.08 (0.48)
$I/\sigma I$	12.3 (2.0)	12.9 (2.2)	10.1 (2.8)	15.3 (2.5)	10.3 (2.1)	7.8 (1.8)
Completeness	99.2% (98.1%)	97.7% (97.8%)	99.2% (98.7%)	97.8% (91.0%)	99.6% (97.7%)	95.2% (91.8%)
Redundancy	4.7 (4.5)	2.2 (2.2)	3.1 (3.1)	5.4 (4.8)	7.7 (7.3)	2.1 (2.0)
Refinement[a]						
Resolution	30 to 1.98 Å (2.02 to 1.98 Å)	36 to 2.6 Å (2.66 to 2.6 Å)	44 to 2.0 Å (2.03–2.0 Å)	58 to 2.0 Å (2.05 to 2.0 Å)	79 to 2.3 Å (2.34 to 2.3 Å)	73 to 2.6 Å (2.66 to 2.6 Å)
No. of reflections	52,797 (2683)	22,615 (2668)	50,034 (1783)	50,456 (3038)	41,466 (2449)	33,200 (2367)
R_{work}/R_{free}	0.19/0.24 (0.32/0.35)	0.23/0.26 (0.32/0.37)	0.18/0.21 (0.24/0.29)	0.19/0.24 (0.28/0.31)	0.21/0.25 (0.31/0.35)	0.19/0.24 (0.26/0.30)
No. of atoms (all)	5802	5522	6226	5776	5701	5198
Protein (chains/residues)	2/678	2/679	2/693	2/689	2/680	2/635
Ligands (sulfate)						5
Water	385	115	667	283	304	78
B-factors						
Protein	47	65	31	34	55	58
Ligands (sulfate)						62
Water	46	45	35	41	42	43
Root mean square deviations						
Bond lengths	0.008 Å	0.01 Å	0.004 Å	0.019 Å	0.021 Å	0.018 Å
Bond angles	1.1°	1.46°	0.82°	1.2°	1.2°	1.5°
Ramachandran statistics						
Residues in favored regions	648 (96.7%)	657 (97.8%)	669 (97.1%)	669 (98%)	650 (97%)	612 (97.6%)
Residues in allowed region	18 (2.7%)	12 (1.8%)	20 (2.9%)	14 (2%)	19 (2.8%)	15 (2.4%)
Residues in outlier region	4 (0.6%)	2 (0.3%)	0 (0%)	0 (0%)	1 (0.1%)	0 (0%)
Crystallization conditions	18% PEG 8000 0.2 M $MgCl_2$ 0.1 M HEPES, pH 7.5	18% PEG 8000 0.2 M $MgCl_2$ 0.1 M HEPES, pH 7	20% PEG 3350 0.2 M $NaNO_3$	20% PEG 3350 0.2 M NaI	20% PEG 3350 0.2 M $NaNO_3$	20% PEG 3350 0.15 M K_2SO_4
Cryo protectant added	15% glycerol	15% glycerol	15% glycerol	20% PEG 400	17% glycerol	15% glycerol
PDB code	4AQN	4ARQ	4ARM	4ARL	4ARP	4ARJ

[a] Values in parentheses are for highest resolution shell.

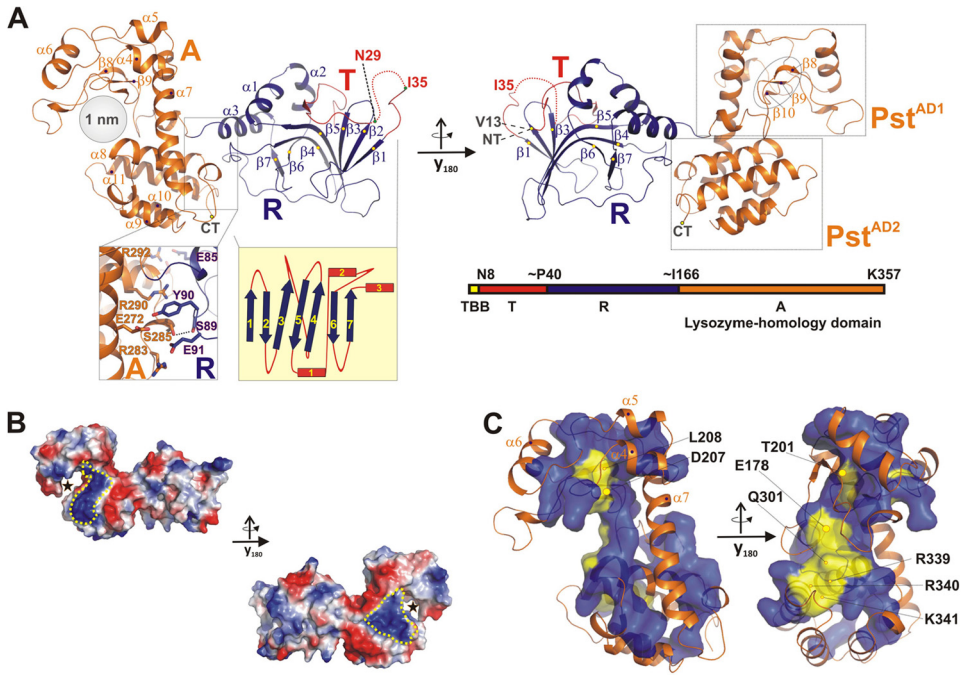

FIGURE 1. **Structural model of pesticin from *Y. pestis*.** *A,* Pst structure in schematic representation is displayed from two different views related to each other by a rotation of 180° around the *y* axis. The N-terminal (*NT*) 12 residues, including the TonB box (*TBB*) and residues 30–34, are not visible in the crystal structure due to disorder. Pst consists of three domains as follow: the translocation domain (*T*), marked in *red*; the receptor binding domain (*R*), marked in *blue,* and the activity domain (*A*), marked in *orange*. The secondary structure assignment is given for β-strands (β1–β8) and α-helices (α1–α11). Two independent Pst^{AD1} and Pst^{AD2} domains connected by α7 helix form the basis of the subdomains of the T4 lysozyme-like structure. The interface residues between the R (*blue*) and A domain (*orange*) are highlighted in the *box below* the structure. One particular hydrogen bond used for the construction of $Pst^{S89C/S285C}$ is marked with *dashed lines*. The R domain includes a mixed α/β-fold, and the A domain is α-helical with three short conserved β-strands (β8–β10, see also Fig. 2*A*). The R domain displays a new fold that is drawn schematically below the structure (β-strands in *blue* and α-helices in *red*). The domain composition together with domain residue boundaries is given in the *schematic bar below* the structures. *B,* surface charge representation of Pst illustrated from the same orientations as in *A*. The active site (marked by a *black star*) is flanked by two patches of positively charged residues that are further surrounded by extended patches of negatively charged residues. *C,* activity domain in the same orientation as *A* is displayed from two sides related by a rotation of 180° around the *y* axis to illustrate conservation of residues. The structure is shown as a schematic model together with the surface representation of conserved (color coded in *blue*) and highly conserved residues (in *yellow*) (see also the alignment in supplemental Fig. S6*B* for comparison). Single residues lining the active site are more strongly conserved and marked with residue type and number. Residues Glu-178, Thr-201, and Asp-207 are particularly important as they form part of the active site (these residues are marked with *large yellow dots*).

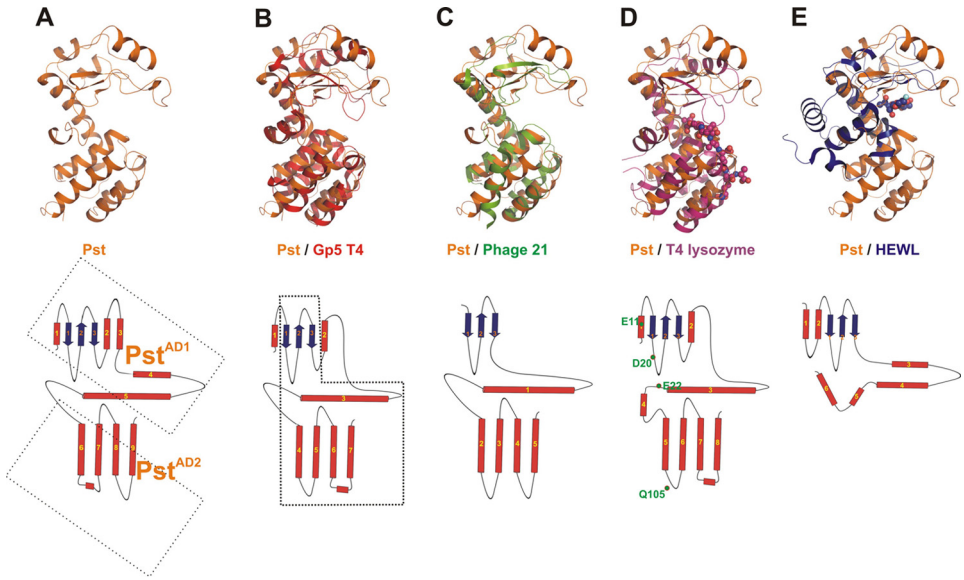

FIGURE 2. **Comparison of the Pst activity domain with lysozyme topology structures.** In the *upper row* the crystal structures of Pst structure alone and structure superpositions (*A*) with the domain of gp5 of bacteriophage T4 (PDB code 1WTH) (*B*), bacteriophage 21 lysozyme (PDB code 3HDF) (*C*), bacteriophage T4 lysozyme (PDB code 148L) (*D*), and HEWL (PDB code 1H6M) (*E*) are shown. In the *bottom row*, the secondary structural topology of the five proteins (based on the DSSP algorithm) are given with β-strands marked in *blue* and α-helices in *red*. *A,* two subdomains forming the activity domain of Pst are encircled by *dashed lines*. *B,* general structure motif of the lysozyme-like molecules excluding HEWL is marked by *dashed lines*. *D,* active site residues of the T4 lysozyme are marked in *green* (Glu-11, Asp-20, and Thr-26). One additional structurally related residue of Pst and T4L mutated in this work is shown.

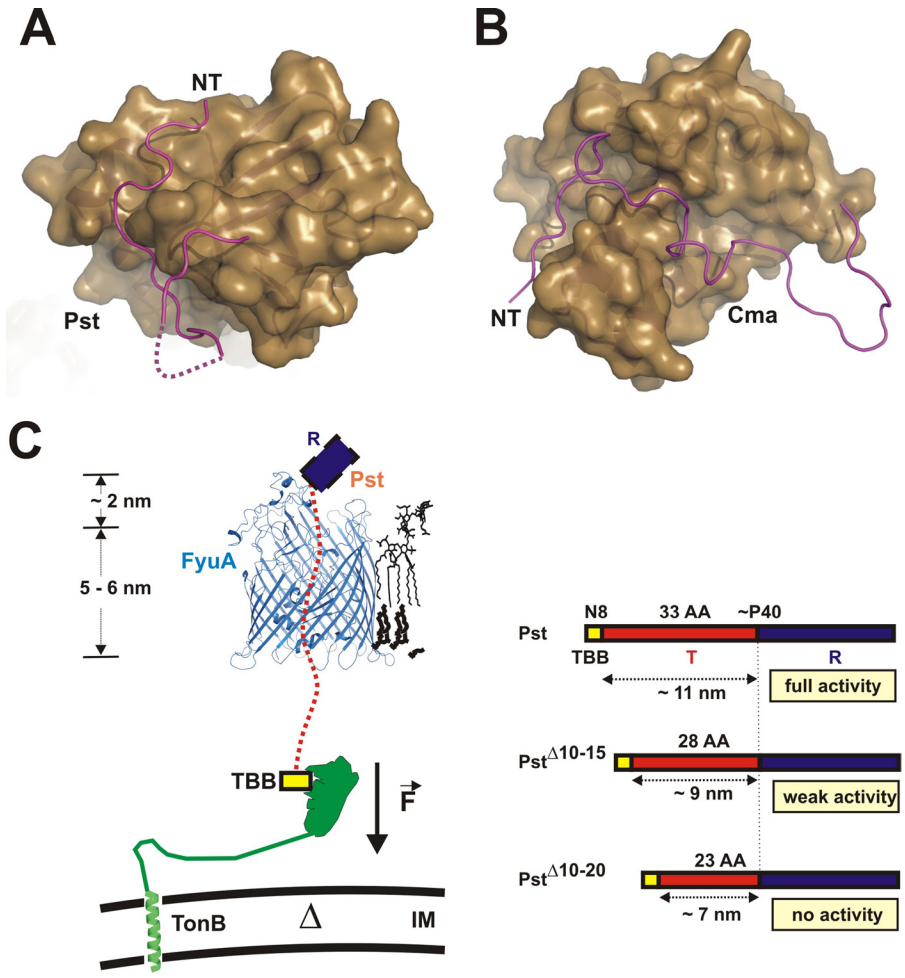

FIGURE 3. **Structure and organization of the translocation domain in bacteriocins.** *A,* surface representation of Pst shown in *sand color* with the T domain shown in schematic form as partially random coil in *magenta* with the N terminus (*NT*) marked. *B,* for comparison, the surface representation of colicin M (*Cma*) in the same schematic drawing as Pst showing the T domain wrapped around the R domain. *C,* model of the translocation of Pst through the FyuA receptor (the structure of FhuA, PDB code 1BY3, was taken as model for FyuA due to the similarity). The distance of the entire membrane-spanning protein is ~9 nm, although the diameter of the membrane spanning part is 5–6 nm. Assuming the T domains of Pst are extended by an artificial force, the terminus could be elongated to ~12 nm. If this terminus is reduced by five residues (~1.5 nm), it would be sufficient to span the membrane and to attach to the periplasmic domain of TonB. A further reduction in length of this domain by another 10 residues (~3 nm) would presumably not allow binding of the bacteriocin to TonB and thereby abolish uptake and *in vivo* activity. The model illustrates the effect of truncation of the T domain on Pst uptake. A schematic representation of the Pst constructs used to determine the importance of the T domain in uptake and activity is given on the *right side*. AA, amino acids; *TBB*, TonB box.

To examine whether the RT domain Pst^{RT} is sufficient for binding to the FyuA receptor, competition of Pst^{RT} with killing by Pst-T4L (see below) was determined. An excess of Pst^{RT} over Pst-T4L inhibited the lytic activity of Pst-T4L in liquid culture (supplemental Fig. S3) as well as in plaque assays (Table 3). This indicates that Pst^{RT} competes with Pst-T4L for binding to the FyuA receptor. Pst^{A} was used as a negative control in the competition assay of which a surplus did not affect the lysis zones formed by Pst-T4L (Table 3).

To study whether the total extension of the T domain has an influence on uptake of Pst, we generated deletions in the T domain adjacent to the TonB box of Pst and tested whether these mutants are still able to interact with the Ton system (Fig. 3*C*). The $Pst^{\Delta 10-15}$ mutant missing residues 10–15 displayed a low activity in the plaque assay forming turbid lysis zones up to a dilution of $1:10^4$ (wild type $1:10^5$), whereas $Pst^{\Delta 10-20}$ missing residues 10–20 was inactive and formed no lysis zones. To examine whether these mutants still bind to FyuA, competition of $Pst^{\Delta 10-20}$ with killing by Pst-T4L was determined. $Pst^{\Delta 10-15}$ showed a residual activity and was therefore unsuitable for the competition assay. In plaque assays, a 5-fold molar excess of $Pst^{\Delta 10-20}$ over Pst-T4L completely prevented formation of a lysis zone by Pst-T4L under conditions by which Pst-T4L gave

TABLE 3

Binding of Pst^{RT}, Pst^{D207A}, and $Pst^{\Delta 10-20}$ proteins to the FyuA receptor determined by competition with Pst-T4L

Pst^{A} was used as a negative control. The numbers indicate the diameters of lysis zones (in mm) that were formed in a plaque assay on LB agar plates seeded with *E. coli* SIP1332 (*fyuA*$^+$) onto which 6 μl of the protein mixture with the molar ratio indicated was applied. The concentration of Pst-T4L was 10 μM. – indicates no lysis zone; turbid lysis zones are given in parentheses, very turbid lysis zones in double parentheses; ND means not determined.

Protein or ratio Pst-T4L:Pst	Pst^{RT}	Pst^{D207A}	$Pst^{\Delta 10-20}$	Pst^{A}
Pst-T4L, no Pst derivative	11	11	11	11
1:2	(8)	(7.5)	ND	11
1:5	((8))	((7.5))	–	11
1:10	–	–	–	11
1:20	–	–	–	11
1:50	–	–	–	11

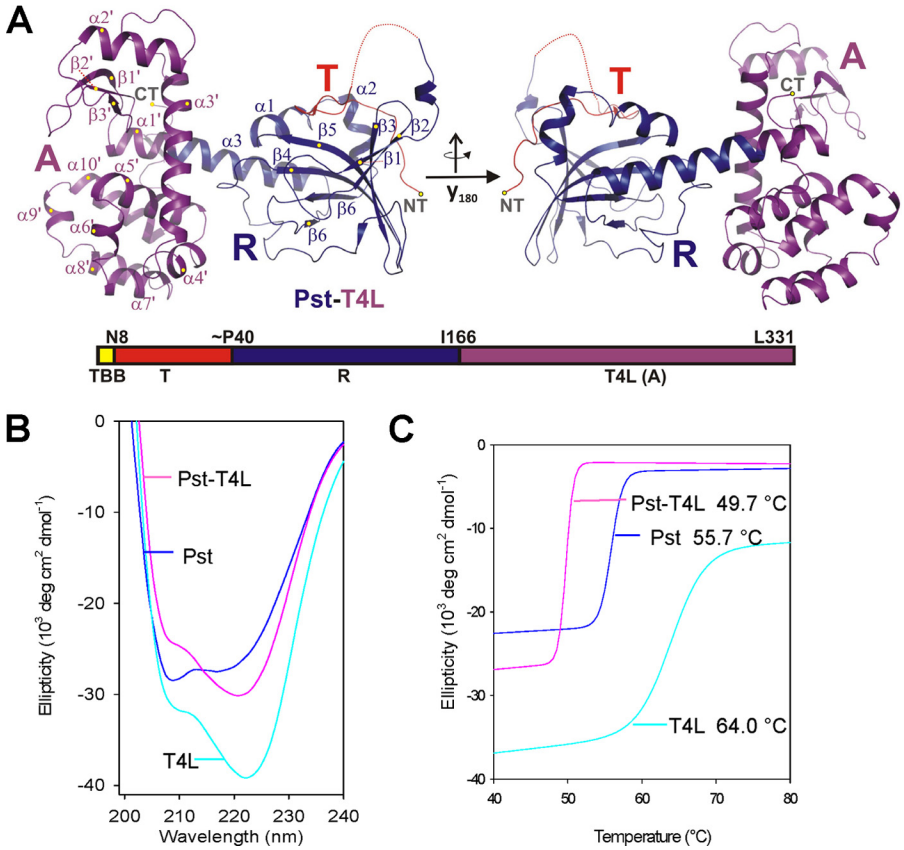

FIGURE 4. **Structure and stability of the Pst-T4L chimera protein.** *A,* chimera structure of the three-domain protein formed by the Pst N-terminal translocation and receptor binding domains (T and R, in *red* and *blue*) and the C-terminal domain, which represents the T4L protein (*A* in *magenta*). The structure is displayed from two points of view related by a rotation of 180° around the *y* axis. The secondary structure assignment essentially follows Fig. 1 for Pst, but the structural elements are individually assigned for the T/R domain ($\alpha1$–$\alpha3$ and $\beta1$–$\beta6$) and the A domain ($\alpha1'$–$\alpha10'$ and $\beta1'$–$\beta3'$). The domain organization (*TBB,* TonB box) also including the boundary residues are marked with *numbers* and represented in the bar-like scheme beyond the structure. *B,* CD spectra; *C,* melting curves of Pst (260 μg/ml), T4L (200 μg/ml), and Pst-T4L (260 μg/ml). The melting temperatures (T_m values) are indicated.

a clear lysis zone of 11 mm (Table 3). Competition with the same concentration of Pst^{RT} or inactive Pst^{D207A} (see below) resulted in turbid lysis zones (Table 3). This suggests that $Pst^{\Delta10-20}$ remains bound to the FyuA receptor, whereas Pst^{RT} and Pst^{D207A} are taken up, and FyuA is cleared. Therefore, higher concentrations of Pst^{RT} and Pst^{D207A} compared with $Pst^{\Delta10-20}$ are necessary to completely block the FyuA receptor for Pst-T4L. The deletion mutant $Pst^{\Delta10-20}$ still binds to FyuA, which can also be inferred for $Pst^{\Delta10-15}$. Assuming the length of the T domain to span the outer membrane receptor plays an important role for the translocation event, we delineated a model on the basis of the Pst, $Pst^{\Delta10-15}$, and $Pst^{\Delta10-20}$ and FhuA (resembling the FyuA) receptor structures (Fig. 3*C*). Assuming that ~33 residues (the T domain reduced by the TonB box residues) are part of the T domain, this elongated protein chain has an approximate extension of 11 nm. Deletion of five residues ($Pst^{\Delta10-15}$) would shorten this construct by 2 nm to 9 nm, whereas deletion of 10 residues would result in an elongated peptide of ~7 nm (Fig. 3*C*). The $Pst^{\Delta10-20}$ mutant has probably been shortened too much to be able to reach the periplasmic TonB. Taking these results together, it appears plausible that the length of the translocation domain is critical for the activity of bacteriocins imported through Ton-dependent uptake receptors.

Plasticity in Bacteriocins, Exchange of the A Domain by T4 Lysozyme Results in an Active Chimera—One of the common features of colicins is their modular architecture composed of T, R, and A building blocks. To examine whether an enzyme that is not derived from bacteriocins can be linked to the RT domain of Pst in a functionally active form and is carried into cells by the RT domain, we replaced Pst^{A} by T4L, which assumes a similar architecture. If the sequence was decisive in translocation across the outer membrane, we expected that Pst-T4L was not transferred into the periplasm because sequence identity to Pst is only 13%. The crystal structure of the fusion protein was solved and showed only small variations to the T and R domain of Pst (Fig. 4*A* and supplemental Fig. S4 for variations). The A domain of Pst-T4L is structurally identical to the open form of T4 lysozyme (PDB code 168L, supplemental Fig. S4). Unexpectedly, the C-terminal helix of Pst^{RT} and the N-terminal helix of T4L form a long continuous connecting helix (Fig. 4*A*). We also collected the CD spectra of Pst, Pst-T4L, and T4L to show that the chimera protein was properly folded in solution (Fig. 4*B*). The melting temperature (T_m) of Pst-T4L (49.7 °C) was significantly lower than that for wild type Pst (55.7 °C) and for T4L (64.0 °C) (Fig. 4*C*). The interface between the R and A domains in Pst is stabilized by 10 hydrogen bonds, whereas this interface is destroyed in the chimera protein. The

R and A domain are aligned relative to each other mostly by the long α-helix and a small contact interface. Although Pst^{RT} and T4L form separate domains in the chimera, the T_m of T4L alone is apparently lowered in the presence of the Pst domain.

To test if the chimera protein was translocated into *E. coli*, we performed plaque assays using genetically constructed *E. coli* strains harboring the FyuA uptake receptor on the surface. Pst-T4L formed a lysis zone on *E. coli* SIP1332 *fyuA*$^+$ and SIP1461 *fyuA*$^+$ *fhuA*$^-$, and no lysis zone on *E. coli* C41 *fyuA*$^-$ and SIP1453 *fyuA*$^+$ *tonB*$^-$ (Table 4). The lysis zones of Pst-T4L were clear compared with slightly turbid lysis zones of Pst. To examine whether Pst-T4L is inhibited by Pim, strain SIP1332 could not be used because the *pim*-plasmid pSP130/33 was not compatible with the *fyuA*-plasmid pSP130/29. Therefore, C41 pHM10 *fyuA*$^+$ was used as an indicator strain. On this strain Pst and Pst-T4L formed lysis zones (Table 4). When the immunity protein Pim was synthesized (C41 pHM10 pSP130/33), only Pst-T4L but not Pst formed a lysis zone, indicating that Pim only protects against Pst and not against Pst-T4L. Although folding of T4L is very similar to that of Pst^A, the different sequence prevents Pim from recognizing T4L. Compared with wild type Pst, Pst-T4L exhibited ~20% *in vivo* activity, because an ~6-fold higher concentration of Pst-T4L than Pst was necessary to give rise to lysis zones of the same size. The results listed in Table 4 show that the chimera protein was imported into the periplasm, and import required the presence of both the FyuA receptor and TonB. The helix connecting Pst^{RT} with T4L may affect different functions, binding to FyuA, unfolding during translocation, refolding in the periplasm, and activity. In fact, Pst-T4L hydrolyzed isolated fluorescein-labeled *Micrococcus lysodeikticus* cell walls with ~10% of the rate of T4L (supplemental Fig. S5).

TABLE 4

***In vivo* activities of Pst-T4L, Pst and T4L**

The numbers indicate the diameters of lysis zones (in mm) that were formed on LB agar plates seeded with the *E. coli* strain indicated onto which 6 μl of 6 μM Pst-T4L, ~1 μM Pst, or 30 μM T4L were spotted. – indicates no lysis zone.

Strain	Protein		
	Pst-T4L	Pst	T4L
C41 (*fyuA*$^-$)	–	–	–
SIP1332 (*fyuA*$^+$)	11	11	–
SIP1453 (*fyuA*$^+$ *tonB*$^-$)	–	–	–
SIP1461 (*fyuA*$^+$ *fhuA*$^-$)	11	11	–
C41 pHM10 (*fyuA*$^+$)	11	11	–
C41 pHM10 pSP130/33 (*fyuA*$^+$ *pim*$^+$)	11	–	–

Disulfide Cross-linking of Structural Motifs Prevents Unfolding and Pesticin Uptake—To test whether unfolding is necessary for uptake of Pst, domains and secondary structural motifs were cross-linked by disulfide bonds. First, we exchanged a serine located in the R domain (S89C) and in close proximity to a serine in the A domain (S285C) by cysteine. These residues are also part of the interface between the R and A domains (Fig. 1*A* and supplemental Fig. S6*A*). Disulfide bond formation was tested by SDS-PAGE whereby the oxidized form has a higher electrophoretic mobility than the reduced form due to the more

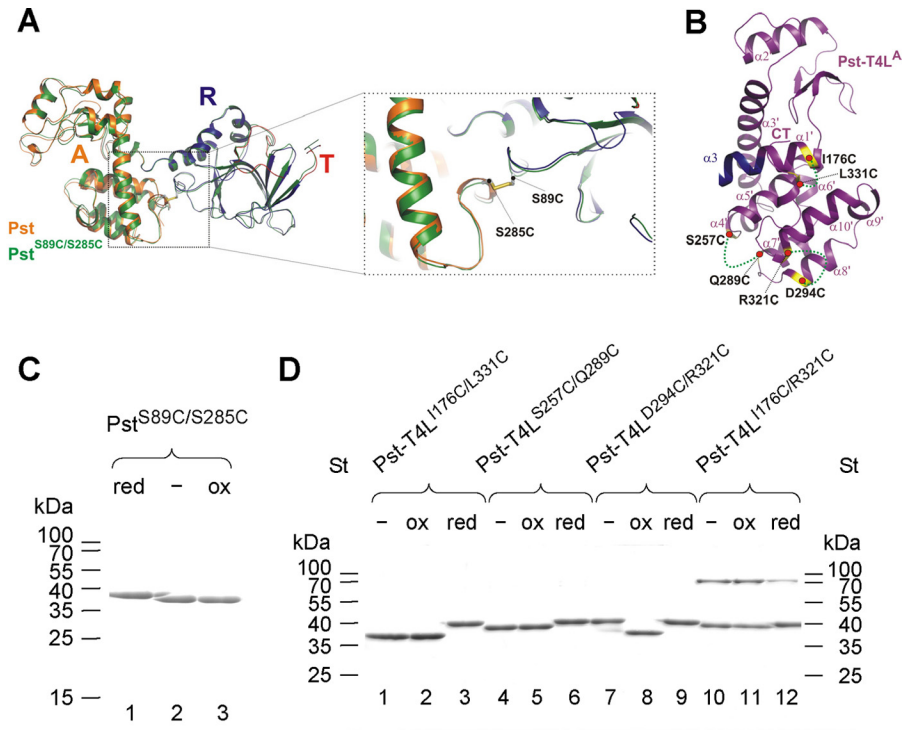

FIGURE 5. **Structure of the covalently linked disulfide derivative of Pst$^{S89C/S285C}$, location of cysteine mutations of Pst-T4L derivatives, and determination of redox state by SDS-PAGE.** *A,* superposition of Pst (*orange*) and the double Cys mutant Pst$^{S89C/S285C}$ in the color coding *red* (T domain), *blue* (R domain), and *green* (A domain). The root mean square deviation between the two structures is 0.55 Å. The *left panel* shows a zoom-in into the structure with the disulfide bond highlighted that connects Pst^R with Pst^A. *B,* location of the residues mutated to cysteines that were used for studies of the redox-dependent uptake of Pst-T4L. Disulfide bonds are displayed as *dashed lines* in the structure of the Pst-T4L activity domain (Pst-T4L^A). *C* and *D,* SDS-PAGE of purified double cysteine derivatives of Pst and Pst-T4L, respectively. Standard proteins were used as molecular weight markers (*St*; Fermentas). The gels were stained with Coomassie Blue. *C,* Pst$^{S89C/S285C}$ oxidized with Cu^{2+} (*ox*, *lane 3*), reduced with 10 mM DTT (*red, lane 1*) or without addition (*lane 2*). *D,* Pst-T4L$^{I176C/L331C}$ (*lanes 1–3*), Pst-T4L$^{S257C/Q289C}$ (*lanes 4–6*), Pst-T4L$^{D294C/R321C}$ (*lanes 7–9*), and Pst-T4L$^{I176C/R321C}$ (*lanes 10–12*), oxidized with Cu^{2+} (*ox*, *lanes 2, 5, 8,* and *11*), reduced with 10 mM DTT (*red, lanes 3, 6, 9,* and *12*), or without addition (*lanes 1, 4, 7,* and *10*).

TABLE 5

***In vivo* activities of oxidized and reduced Pst-T4L and Pst disulfide derivatives**

The numbers indicate the diameters of lysis zones (turbid lysis zones in parentheses) that were formed on LB agar plates seeded with the pesticin-sensitive *E. coli* strain SIP1322 *fyuA*$^+$ onto which 6 μl of serial 10^1- to 10^5-fold dilutions of pesticin solutions were placed. The concentration of the stock solution was 10 μM for Pst-T4L wild type and derivatives and 2 mM for Pst wild type and derivatives. – indicates no lysis zone.

Protein	Dilution				
	1:10^1	1:10^2	1:10^3	1:10^4	1:10^5
Pst-T4L wild type	11	9	6.5	(5)	–
Pst-T4L wild type + DTT	11	9	6.5	(5)	–
Pst-T4L wild type + Cu^{2+}	11	9	6	(5)	–
Pst-T4L$^{I176C/L331C}$	–	–	–	–	–
Pst-T4L$^{I176C/L331C}$ + DTT	11	9.5	7.5	(5)	–
Pst-T4L$^{S257C/Q289C}$	–	–	–	–	–
Pst-T4L$^{S257C/Q289C}$ + DTT	10	8	(8)	–	–
Pst-T4L$^{D294C/R321C}$	10	8	6	(5)	–
Pst-T4L$^{D294C/R321C}$ + DTT	10	8	6	(5)	–
Pst-T4L$^{D294C/R321C}$ + Cu^{2+}	(10)	–	–	–	–
Pst-T4L$^{I176C/R321C}$	9	(7.5)	–	–	–
Pst-T4L$^{I176C/R321C}$ + DTT	9	7.5	(6)	–	–
Pst wild type	16	14.5	12	10	7
Pst$^{S89C/S285C}$	–	–	–	–	–
Pst$^{S89C/S285C}$ + DTT	16.5	15	13	10.5	8

compact structure. The mutant protein became oxidized during purification, and disulfide bonds were spontaneously formed (Fig. 5*C*). When the cysteine bridges were reduced with DTT, the protein showed a slower electrophoretic mobility (Fig. 5*C*). The crystal structure of the oxidized form determined at 2.6 Å resolution was identical to the wild type protein with a small deviation between main chain atoms of 0.8 Å root mean square deviation (Fig. 5*A*). In the oxidized form, the protein was inactive in the plaque assay and did not form lysis zones (Table 5). The reduced protein displayed the same activity as wild type Pst. Lysis zones up to a 10^5-fold dilution were observed on agar plates seeded with *E. coli* SIP1332 *fyuA*$^+$ (Table 5).

To examine whether small subdomains (*e.g.* two α-helices) must unfold for Pst uptake, intra-domain cysteine mutant pairs were prepared. For these studies the T4L domain of the Pst-T4L chimera was selected, because *in vitro* hydrolysis of PG by the disulfide mutant proteins could be tested, which cannot be done with Pst, which *in vitro* is inactive. In addition, we could rely on the structure and stability information of disulfide mutants of T4 lysozyme previously determined in the group of Matthews and co-workers (31). Like Pst, the Pst-T4L construct does not contain cysteines (the cysteines of T4 lysozyme were mutated to alanine and threonine). To examine whether disulfide bonds were formed, the Pst-T4L mutant proteins were isolated, purified, and applied to SDS-PAGE (Fig. 5*D*). The two cysteine residues in Pst-T4L$^{I176C/L331C}$ are localized at the N and C termini of the T4L domain, and the cysteine residues in Pst-T4L$^{S257C/Q289C}$ are located at the C-terminal ends of helices α4 and α7 (Fig. 5*B*). Isolated Pst-T4L$^{I176C/L331C}$ and Pst-T4L$^{S257C/Q289C}$ showed an electrophoretic mobility that was not altered upon incubation with Cu^{2+} to oxidize cysteines. After incubation with DTT and reduction of the disulfide bond, the proteins showed a lower electrophoretic mobility (Fig. 5*D*). These data indicate that the two proteins quantitatively formed disulfide bonds during isolation. In contrast, Pst-T4L$^{D294C/R321C}$ with the cysteines in two parallel helices α8 and α10 moved into the position of the reduced form and transformed into the oxidized form upon incubation with Cu^{2+}. After incubation with DTT, the protein shifted back to the open form with retarded mobility. This protein did not spontaneously form disulfide bridges, but the cysteines were located sufficiently close enough that Cu^{2+} induced disulfide bond formation. A fourth double mutant Pst-T4L$^{I176C/R321C}$ was constructed as control with both mutated residues located far apart from each other, and intramolecular disulfide bond formation was not expected. In SDS-PAGE, the protein was primarily located at the position of the reduced form, but a small portion moved slower at the position corresponding to the cross-linked protein dimer (Fig. 5*D*). The formation of a stable structure after cross-linking was examined by determination of the melting temperatures. Although the Pst-T4L chimera showed a transition state temperature of 49.7 °C both under reducing and oxidizing conditions, Pst-T4L$^{I176C/L331C}$ showed unfolding at 53.4 °C in the oxidized form and at 49.4 °C in the reduced form. In comparison, Pst-T4L$^{S257C/Q289C}$ was unfolded at 50.0 °C in the oxidized form and at 47.6 °C in the reduced form (supplemental Fig. S7).

To examine the activities of the disulfide derivatives, 10-fold serially diluted protein solutions were spotted onto nutrient agar plates seeded with *E. coli* SIP1332 *fyuA*$^+$. As expected, both oxidized Pst-T4L$^{I176C/L331C}$ and Pst-T4L$^{S257C/Q289C}$ constructs did not inhibit cell growth (Table 5). Upon reduction with DTT, Pst-T4L$^{I176C/L331C}$ expressed the same activity as wild type Pst-T4L, whereas Pst-T4L$^{S257C/Q289C}$ showed a 10-fold lower but still significant antimicrobial activity (Table 5). The constructs harboring disulfide bonds were inactive in the oxidized form and became active after reduction to cysteines. In contrast, Pst-T4L$^{D294C/R321C}$ showed the same activity as wild type Pst-T4L but became inactive upon incubation with Cu^{2+}. This mutant did not spontaneously form disulfide bridges, and oxidation by Cu^{2+} was required. In the three mutant proteins tested, disulfide bond formation hampered unfolding of the A domain, which rendered the cross-linked mutants inactive. Pst-T4L$^{I176C/R321C}$ showed residual activity which upon reduction was 10-fold increased. Introduction of the cysteines led to an aberrant form (dimer), and the wild type structure was not fully restored upon reduction.

To examine whether introduction of cysteine residues and formation of disulfide bonds did not influence the activity of the T4L domain, the *in vitro* activity of oxidized Pst-T4L$^{I176C/L331C}$ and Pst-T4L$^{S257C/Q289C}$ was tested with fluorescently marked cell walls of *M. lysodeikticus*. Both derivatives showed activities in the range of Pst-T4L activity (shown in supplemental Fig. S5 for Pst-T4L$^{I176C/L331C}$). The data clearly show an unaltered enzymatic activity of the disulfide-linked Pst-T4L proteins, which excluded that disulfide bond formation inactivated their active sites. The data indicate that cross-linking of the R domain with the A domain and cross-linking within the A domain prevents unfolding and as a consequence uptake of Pst and Pst-T4L into the periplasm.

Pst and the Pst Activity Domain Kill Cells if Imported from the Cytoplasm—Bacteriocins like colicin M and Pst predominantly remain in the cytoplasm because their operons do not encode lysis proteins for release of the bacteriocins. For colicin M it has been shown that the colicin must be imported to kill cells (32). To test if Pst when secreted from the cytoplasm into the

periplasm by the Sec machinery can degrade PG, we fused Pst and its activity domain Pst^{A} to the signal peptide of the MalE periplasmic binding protein. The genes were cloned downstream of the *ara* promoter that tightly controls transcription of downstream genes. In addition, glucose represses transcription. This was important for cloning because noninduced basal levels of *pst* transcription might have resulted in the failure to obtain transformants because of cell lysis. In addition, the level of expression can be adjusted with arabinose up to 1200-fold (33). As controls, we chose the proteins without signal sequence and the *in vivo* inactive Pst^{E178A} mutant. Cells were grown either in the presence of 0.2% glucose or with various concentrations of arabinose to induce transcription. Lysis was determined by quantification of the absorbance of growing cultures. Because MalE′-Pst lysed cells already without induction at 37 °C, cells were cultured at 30 °C in the presence of 0.2% glucose. Under these conditions, cells stopped growing but did not lyse (Fig. 6*A*). Expression of MalE′-Pst and induction of cell lysis were differentially induced and monitored through addition of 0.0001 to 0.1% arabinose. Cells lysed already when grown in the presence of 0.001% arabinose (Fig. 6*A*). A qualitatively similar result was obtained with MalE′-Pst^{A}, which lysed cells in the presence of 0.1% arabinose; 0.01% arabinose stopped growth and 0.001% retarded growth. MalE′-Pst^{A} secreted via the Sec system into the periplasm killed cells but was less effective than MalE′-Pst (Fig. 6*B*). Compared with MalE′-Pst, less of the synthesized MalE′-Pst^{A} is processed (MalE signal sequence cut off) and exported into the periplasm as shown by Western blotting of MalE′-Pst^{E178A} and MalE′-Pst$^{A\ E178A}$, which do not lyse cells (see below), and immunodetection with a monoclonal anti-His tag antibody (data not shown). This might be due to a higher propensity of Pst^{A} than Pst to form inclusion bodies in the cytoplasm (see under "Experimental Procedures"). The controls, Pst and Pst^{A} without MalE signal sequence (data not shown) as well as MalE′-Pst^{E178A} and MalE′-Pst$^{A\ E178A}$ carrying an active site mutation, did not lyse cells (Fig. 6, *A* and *B*). The A domain apparently folds in the periplasm to an active domain, and folding does not require the RT domain. Import across the outer membrane via FyuA, TonB, ExbB, and ExbD is not required.

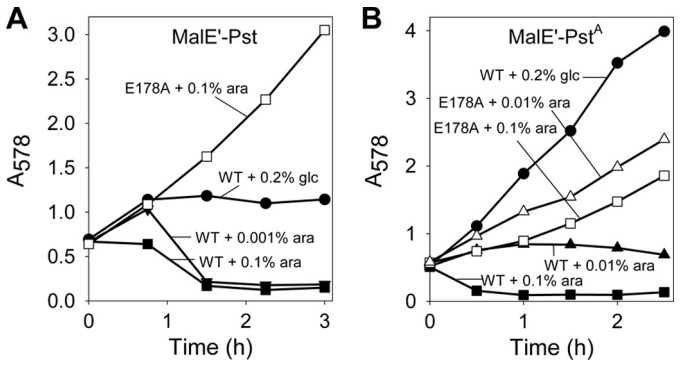

FIGURE 6. *A,* growth curves of *E. coli* DH5α transformed with plasmids that encode wild type Pst fused to the MalE signal sequence at 30 °C. Transcription was induced with 0.1% arabinose (■) and 0.001% arabinose (▼) or repressed by 0.2% glucose (*glc*) (●). Cells transformed with the mutated MalE′-Pst^{E178A} plasmid were not inhibited after induction with 0.1% arabinose (□). *B,* growth curves of *E. coli* SIP1332 *fyuA*$^{+}$ transformed with plasmids that encode Pst^{A} fused to the MalE signal sequence at 37 °C. Transcription was induced with 0.1% arabinose (■), 0.01% arabinose (▲), or repressed by 0.2% glucose (●). Cells transformed with the mutated MalE′-Pst$^{A(E178A)}$ plasmid were not lysed after induction with 0.1% arabinose (□) and 0.01% arabinose (Δ).

Investigation of the Active Site of Pesticin—Pst^{A} and T4 lysozyme show a very similar fold and the same enzymatic activity. To further characterize the active center of Pst, we employed structural analysis, sequence comparison (Fig. 7*A*), and mutant analysis. Based on the extensive studies by Matthews and co-workers (34, 35) who identified Glu-11, Asp-20, and Thr-26 as key residues for enzymatic activity, we selected equivalent residues in Pst. Pairwise sequence and structural alignment of the two proteins only partially matched due to the

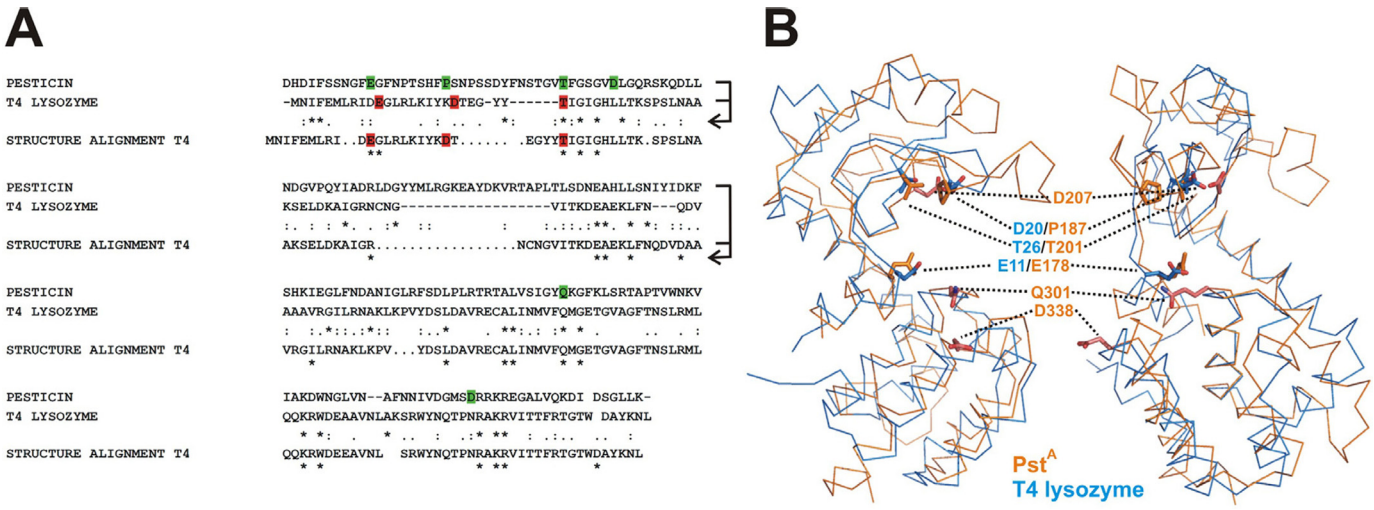

FIGURE 7. **Tracing the active center of Pst using point mutants.** *A,* sequence and structural alignment of the activity domain of Pst and T4 lysozyme. In the sequence alignment (*lines 1–3*), the identical residues are marked with *asterisk*, strongly conserved residues are marked with *colon*, and weakly conserved residues are marked with *period*. In the structural alignment, only the identical positions (within a root mean square deviation of 3.5 Å between Cα positions) are marked (*). Residues mutated in Pst for activity assays are marked in *green*. Active site residues in T4 lysozyme are highlighted in *red*. *B,* superposition of the structures of Pst^{A} and T4 lysozyme (PDB code 168L) in ribbon representation in two orientations (*left* and *right*). Residues chosen for mutagenesis according to the structure and sequence alignment were mutated into alanines (see also *A*). These residues are marked as *sticks* together with residue and number for Pst and compared with identical T4 lysozyme positions (T4 lysozyme/Pst). Additional residues mutated in Pst are marked by *sticks* and residue numbers (Asp-207, Gln-301, and Asp-338).

TABLE 6

Activities of Pst and its predicted active site derivatives

The numbers indicate the diameters of lysis zones (in mm) that were formed on LB agar plates seeded with the pesticin-sensitive *E. coli* strain SIP1322 *fyuA*$^+$ onto which serial 20 μl of 10^1- to 10^6-fold dilutions of pesticin solutions (2 mM) were placed. – indicates no lysis zone.

	Dilution					
Protein	**1:10^1**	**1:10^2**	**1:10^3**	**1:10^4**	**1:10^5**	**1:10^6**
Pst^{WT}	20	17	15	14	10	–
Pst^{E178A}	–	–	–	–	–	–
Pst^{P187A}	14	14	11	10	–	–
Pst^{T201A}	–	–	–	–	–	–
Pst^{D207A}	–	–	–	–	–	–
Pst^{Q301A}	16	15	14	12	–	–
Pst^{D338A}	20	17	15	14	10	–

low sequence identity of the proteins (13%). Mutants based on the alignments of Pst with Pst homologs (supplemental Fig. S6*B*) seemed to be more reliable for active site determination. Glu-178, Pro-187, and Thr-201 were selected for alanine substitutions because they are located in the predicted active center (Fig. 7*A*). Asp-207 was selected due to its proximity to the active site (Fig. 7, *A* and *B*) (35), and Gln-301, although distant from the active site, corresponds to Gln-105 of T4L. Asp-207 in Pst has no functionally conserved residue in T4L but may resemble Asp-20 of T4L because it is the only Asp residue in proximity to Glu-178 in Pst. Finally, Pst^{D338A} was constructed as a negative control because this residue is an Asp residue apart from the active site (Fig. 7*B*). Mutant proteins were purified to electrophoretic homogeneity (supplemental Fig. S1*B*), and the activities of the resulting derivatives were tested *in vivo*. 10-Fold serial dilutions of the purified proteins were spotted on nutrient agar plates seeded with *E. coli* SIP1322 carrying the plasmid-encoded *fyuA* gene that conferred sensitivity to Pst. The wild type Pst and Pst^{D338A} solution could be diluted up to 10^5-fold to yield clear lysis zones (Table 6). In contrast, Pst^{E178A}, Pst^{T201A}, and Pst^{D207A} were completely inactive, whereas Pst^{P187A} and Pst^{Q301A} displayed 10% of wild type activity. The mutations did not alter the overall structure of the mutant proteins, as revealed by the CD spectra that were identical to wild type Pst (supplemental Fig. S8*B*) and by determination of the crystal structures (supplemental Fig. S8*A*). The melting temperatures T_m of Pst^{E178A}, Pst^{P187A}, Pst^{T201A}, Pst^{Q301A}, and Pst^{D338A} were similar to the T_m of wild type Pst (supplemental Fig. S8*C*), whereas the T_m value for Pst^{D207A} was ~4 °C lower. To verify that the inactive proteins were not impaired in binding to FyuA, competition with killing by Pst-T4L was determined for Pst^{D207A} as an example. At a 10-fold molar excess over Pst-T4L, Pst^{D207A} completely prevented lysis zone formation (Table 3), indicating that it binds FyuA.

PG hydrolysis of the Pst mutant proteins could not be tested *in vitro* by hydrolysis of *E. coli* spheroplasts, *M. lysodeikticus* cells, and fluorescein-labeled *M. lysodeikticus* cell walls, because Pst was inactive in these assays. However, these substrates were rapidly hydrolyzed by HEWL and isolated T4L (see above for fluorescein-labeled *M. lysodeikticus* cell walls). The failure to hydrolyze these substrates agrees with the known low enzymatic activity of pesticin (3, 4).

DISCUSSION

Bacteria compete with closely related bacteria of the same niche by secretion of toxins into the external space. In natural *E. coli* cultures, a significant number of roughly 50% of bacteria harbor plasmids that encode a variable number of colicins, immunity proteins, and lysis proteins produced to allow for the improved release into the external medium (1). Although bacteriocins of the colicin type have been intensively studied for many years, related proteins from pathogenic bacteria remained enigmatic, although protein toxins from many pathogenic bacteria, including *Vibrio cholerae*, *Pseudomonas aeruginosa*, *Salmonella typhimurium,* and *Y. pestis*, for example, have been described in the literature. Recently, the application of engineered *E. coli* strains secreting pyocin was shown to inhibit the formation of biofilms, and killing of pathogenic *P. aeruginosa* was demonstrated (36). Further possible applications of bacteriocins in targeting pathogenic bacteria also require studies as to the mechanisms by which these molecules become active to improve targeting strategies in the future.

Yersinia bacteria harbor small plasmids that encode pesticin as the unique anti-microbial weapon. These anti-bacterial proteins are similar in function to other toxins or antibiotics but act more specific against a subset of closely related bacteria. By contrast to small anti-microbial agents (peptides and chemicals), bacteriocins misuse existing transport systems for substrates via outer membrane receptors coupled either to the Ton or Tol systems to kill bacteria in their vicinity. To understand the mechanism by which pesticin from *Y. pestis* mechanistically acts on related bacteria, we have analyzed its crystal structure and found a similar domain organization as known for colicins. Three structurally separated domains, the N-terminal translocation domain, the receptor binding domain, and the C-terminal activity domain, are present. This architecture is archetypical for most bacteriocins.

The structure of pesticin revealed several unexpected features. Subdivision of colicins into domains is sometimes apparent from the structural or sequence analysis. In Pst, the RT domain forms one entity and the A domain another compact structured domain that are linked by a short unstructured linker. In many colicin structures the A domains are well separated from the R and T domains, although this rule does not apply to colicin M, for example. In some colicins, *e.g.* E3 and Ia, the R and T domains form separate folds, whereas in colicins B, M, and S4 (37), the T domains are less structured and form flexible regions that are prone to unfold during import across the outer membrane (1). In a structural homology search, domains similar to Pst appeared only for the A domain that shows a structure similar to phage proteins (Fig. 2). Despite the low sequence identity of 13% between Pst and T4 lysozyme, the Pst A domain folds similarly into two domains (A_{D1} and A_{D2}, equivalent to the N- and C-terminal domain in T4 lysozyme) with small structural deviations due to insertions in the sequence. So far, none of the bacteriocin A domains (DNases, RNases, or phosphatases) displayed an overall structure similarity to existing enzymes. Although the sequence identity to T4 lysozyme is low, there is a clear sequence relationship between the Pst A domain and the related lysozymes. Therefore, it is

tempting to speculate that one of the phage lysozymes formed the evolutionary precursor of Pst (supplemental Fig. S2). Although shuffling of DNA fragments encoding R, T, or A domains is a major driving force for the evolution of colicins (38–40), the exchange of DNA fragments was observed among colicins but not with chromosomal genes, phage genes, and plasmid-encoded genes outside colicin loci. Pst may be the first representative of this kind. By contrast to the A domain, neither the T nor the R domain show any significant sequence relationship to known proteins and may have specifically evolved to bind to the import receptor. This is typical for several colicins, including colicin M, for which related activity domains exist but the T and R domains are unique (29).

Pesticin is unique for additional reasons, one of which is degradation of PG. This periplasmic activity of pesticin is shared so far only with colicin M from *E. coli*, although this protein acts as phosphatase on the lipid-linked biosynthetic precursor of PG. Both bacteriocins bind and translocate via iron siderophore receptors, FhuA for colicin M and FyuA for pesticin. In analogy to colicin M, Pst harbors an elongated and unstructured T domain with an approximate length of 40 residues. Another example is colicin B, which is recognized and translocated through the FepA iron receptor (30). This colicin also comprises a long unfolded and partially unstructured N-terminal domain of ~60 residues, which is slightly longer than that of Pst or colicin M. The T domains are firmly attached to the protein and wrap around the R domain of the bacteriocin species (Fig. 3, *A* and *B*). The length of these extensions if elongated is sufficient to span the entire receptor of ~ 8 nm and to attach to the periplasmic TonB protein. If the length of the Pst N terminus is reduced by 5 or 10 residues, while keeping the TonB box motif intact as prerequisite for translocation, the activity of the protein is reduced or abolished.

To test the plasticity of Pst, we exchanged the structurally well separated A domain and replaced it by T7 and T4 lysozymes to examine whether these chimera killed *E. coli* cells. Although overexpressed Pst-T7 lysozyme was inactive, the Pst-T4L fusion was active, and import was demonstrated. The Pst-T4L hybrid protein caused clear lysis zones on nutrient agar plates seeded with a pesticin-sensitive *E. coli* strain and lysed cells in liquid culture. The high activity of Pst-T4L indicated the efficient uptake into the periplasmic space via the RT domain and the FyuA receptor. Given the low sequence similarities between T4 lysozyme and Pst^{A}, the uptake of the A domain across the outer membrane apparently has no or little sequence specificity. Nevertheless, it appears plausible that for the directed import into the periplasm, involving unfolding and refolding, the structure of the protein may need to resemble the structure of Pst^{A}, as is the case for T4L. Both domains unfold already under relatively moderate conditions (T_m ~50 °C), which may be a prerequisite for their successful import via the Pst RT domain. Pst-T4L killed cells less effective than Pst (size of the lysis zones in plaque assays). The lower *in vivo* activity may be caused by a less efficient translocation across the outer membrane for which Pst^{A} was optimized during evolution but not T4L. In particular, the unfolding rate may be reduced by the α-helix that connects the Pst RT domain with T4L. In contrast to T4L, pesticin did not hydrolyze isolated fluorescein-labeled PG of *M. lysodeikticus*. This *in vitro* assay can be used to discriminate between T4L and Pst activity, and the data argue for a difference in the active site of T4L and Pst. We also tried this assay at pH 4.7, which is reported to be the optimum for Pst activity (41), and with addition of Ca^{2+}, but Pst did not hydrolyze the substrate. It might be that the difference in peptide side chains of PG of *M. lysodeikticus* compared with PG of *E. coli* or a steric hindrance due to the fluorescein labeling of amino groups account for this. However, also *E. coli* PG is hydrolyzed only slowly. In former experiments, radiolabeled *E. coli* PG was incubated up to 5 h with a 6-fold higher concentration than HEWL to identify the cleavage site of Pst (4). The low PG hydrolase activity seems to be sufficient to kill *E. coli* cells. We consider it as less likely that in addition to PG hydrolysis Pst disrupts PG biosynthesis by binding to PG or that an additional factor in the periplasm enhances the Pst hydrolysis rate. Rapid killing of cells despite formation of stable spheroplasts in the absence of osmotically stabilizing sucrose indicates a special mode of action based on slow PG hydrolysis.

Although T4L folds like Pst^{A} and has the same enzymatic activity, it is not recognized by the Pst immunity protein Pim. The sequences of Pst and T4L are not sufficiently similar that Pim binds to T4L. Lack of inactivation shows that Pim binds preferentially to Pst^{A} and that the RT domain plays no major role. However, the helix connecting Pst^{RT} with T4L may also interfere with Pim binding.

Proteins typically need to unfold during their passage across membranes. This has been demonstrated for the bacterial inner membrane and the outer membrane of mitochondria. However, the extent of unfolding has not been clearly determined, and it has been reported that the TOM complex of the mitochondrial membrane allows for the passage of small and folded secondary structural elements. To examine to what extent Pst needs to be unfolded, we introduced disulfide bridges between domains of Pst and between secondary structural elements of the activity domain of the Pst-T4L chimera and monitored the redox-dependent activity *in vivo* and *in vitro*. The oxidized forms of these proteins were completely inactive, but activity could be recovered upon reduction through reducing agents. To exclude that the cross-links inactivated the lysozyme domain, two of the oxidized and reduced forms were incubated *in vitro* with PG. Both forms displayed activities similar to wild type Pst-T4L. Inactivity of the disulfide cross-linked derivatives was not caused by inactivation of the lysozyme. Rather, the cross-linked derivatives were impaired in uptake because unfolding was prevented. Evidence for unfolding of colicins during import has been obtained by various techniques, such as disulfide cross-linking of colicins (42–44), FRET analysis of labeled colicin (45), competition between colicins (46), and identification of the released A domain (nuclease) in the cytoplasm (47). Thus, interpretation of the cross-linking data of Pst-T4L is in agreement with previous results on related colicins (see also Discussion in Ref 48). Although we expected incremental differences in activity due to distinct unfolding properties of the disulfide mutants, the total lack of activity indicates that the uptake system does not tolerate cross-linking of domains and subdomains, even if structurally neighboring helices are concerned. Presumably, the diameter of the uptake

receptor barrel restricts the simultaneous translocation of (partially) folded secondary structural elements. This does not exclude that helices remain folded during their passage through the uptake channel.

Colicins that are co-expressed with a lysis protein are not released from cells by specific export systems but by quasi-lysis of the cell membranes. Colicins without this lysis protein remain inside cells (1). The lack of a lysis protein retains more than 90% of Pst inside producer cells. We asked whether Pst and its A domain equipped with a signal sequence were secreted by the Sec apparatus from the cytoplasm into the periplasm. Unfolded proteins are secreted by Sec and must refold in the periplasm to be active in this compartment. We tested cell lysis at various protein expression levels. Pst and the Pst A domain lysed cell, which means that they were secreted and refolded. Secretion across the cytoplasmic membrane supports the ability of Pst to unfold during import across the outer membrane. The Pst activity domain folds in the periplasm without the help of the RT domain.

Although the same bond in PG is hydrolyzed by Pst and T4L, the catalytic mechanism may be slightly distinct because residues in the predicted active center of Pst differ from residues known to contribute to PG binding and hydrolysis of T4L (Fig. 7*B*) (49, 50). Five residues of Pst were replaced by alanine, and the activity of the resulting proteins was determined by inspecting lysis of cells on nutrient agar plates. Three of the proteins (Pst^{E178A}, Pst^{T201A}, and Pst^{D207A}) were inactive. Two of the residues (Glu-178 and Thr-201) are structurally conserved between Pst and T4 lysozyme. Two mutants (Pst^{P187A} and Pst^{Q301A}) showed a 10-fold reduced activity. Apart from Gly, Ala, and Leu, Glu-178, Pro-187, Thr-201, Asp-207, and Gln-301 are the only residues that are strictly conserved throughout all sequences in an alignment of Pst with Pst homologs (supplemental Fig. S6*B*). The inactive mutants may define residues involved in hydrolysis, whereas the partially active mutants may affect residues that bind the substrate or affect folding.

CONCLUSIONS

This paper describes for the first time the structure of a bacteriocin that kills cells by degrading PG. Determination of the crystal structure of Pst revealed a similar fold to T4 lysozyme and lysozyme homologs. This finding is somewhat surprising as lysozymes have very different sequences, and no colicin up to now resembled the structure of another known enzyme fold. We showed that the length of the T domain is important for uptake. Furthermore, the replacement of Pst^{A} by T4L yielded a functional toxin that was taken up across the outer membrane by the RT domain. This result allows a number of future studies with respect to the general plasticity of import mechanisms (*e.g.* domain size, stability) and may in principle allow the import of other bacterial and nonbacterial proteins. The cross-linking data indicate that Pst and Pst-T4L need to unfold during import into the periplasm. Moreover, unfolded Pst and Pst^{A} fused to a signal sequence are secreted from the cytoplasm into the periplasm by the Sec translocase and fold in the periplasm to an active toxin. Translocation across the outer membrane differs from translocation across the cytoplasmic membrane. Folding of the A domain to the active toxin occurs in the periplasm regardless of whether the RT domain is present or not. Both Pst and Pst^{A} did not hydrolyze *M. lysodeikticus* cell walls. This low *in vitro* hydrolysis is an intrinsic property of Pst. Finally, we identified the active site residues of Pst that are similar but not identical to those of T4 lysozyme, and we revealed additional amino acids previously not identified that influence Pst activity.

Acknowledgments—V. B. and S. I. P. thank Andrei N. Lupas for generous hospitality and discussion. Thomas Ellinghaus and Niklas Hoffmann made initial contributions to this work. We thank the entire beamline staff of PXII at the Swiss Light Source (SLS) for beamline maintenance and continuous support.

REFERENCES

1. Cascales, E., Buchanan, S. K., Duché, D., Kleanthous, C., Lloubès, R., Postle, K., Riley, M., Slatin, S., and Cavard, D. (2007) Colicin biology. *Microbiol. Mol. Biol. Rev.* **71,** 158–229
2. Schaller, K., Höltje, J. V., and Braun, V. (1982) Colicin M is an inhibitor of murein biosynthesis. *J. Bacteriol.* **152,** 994–1000
3. Hall, P. J., and Brubaker, R. R. (1978) Pesticin-dependent generation of somotically stable spheroplast-like structures. *J. Bacteriol.* **136,** 786–789
4. Vollmer, W., Pilsl, H., Hantke, K., Höltje, J. V., and Braun, V. (1997) Pesticin displays muramidase activity. *J. Bacteriol.* **179,** 1580–1583
5. Pilsl, H., Killmann, H., Hantke, K., and Braun, V. (1996) Periplasmic location of the pesticin immunity protein suggests inactivation of pesticin in the periplasm. *J. Bacteriol.* **178,** 2431–2435
6. Kurisu, G., Zakharov, S. D., Zhalnina, M. V., Bano, S., Eroukova, V. Y., Rokitskaya, T. I., Antonenko, Y. N., Wiener, M. C., and Cramer, W. A. (2003) The structure of BtuB with bound colicin E3 R domain implies a translocon. *Nat. Struct. Biol.* **10,** 948–954
7. Sharma, O., Yamashita, E., Zhalnina, M. V., Zakharov, S. D., Datsenko, K. A., Wanner, B. L., and Cramer, W. A. (2007) Structure of the complex of the colicin E2 R domain and its BtuB receptor. The outer membrane colicin translocon. *J. Biol. Chem.* **282,** 23163–23170
8. Buchanan, S. K., Lukacik, P., Grizot, S., Ghirlando, R., Ali, M. M., Barnard, T. J., Jakes, K. S., Kienker, P. K., and Esser, L. (2007) Structure of colicin I receptor bound to the R-domain of colicin Ia: implications for protein import. *EMBO J.* **26,** 2594–2604
9. Jakes, K. S., and Finkelstein, A. (2010) The colicin Ia receptor, Cir, is also the translocator for colicin Ia. *Mol. Microbiol.* **75,** 567–578
10. Rakin, A., Boolgakowa, E., and Heesemann, J. (1996) Structural and functional organization of the *Yersinia pestis* bacteriocin pesticin gene cluster. *Microbiology* **142,** 3415–3424
11. Sambrook, J., and Russell, D. W. (2001) *Molecular Cloning: A Laboratory Manual*, 3 Ed., Cold Spring Harbor Laboratory Press, Cold Spring Harbor, NY
12. Helbig, S., Patzer, S. I., Schiene-Fischer, C., Zeth, K., and Braun, V. (2011) Activation of colicin M by the FkpA prolyl cis-trans isomerase/chaperone. *J. Biol. Chem.* **286,** 6280–6290
13. Papworth, C., Bauer, J. C., Braman, J., and Wright, D. A. (1996) Site-directed mutagenesis in 1 day with >80% efficiency. *Strategies* **9,** 3–4
14. Hanoulle, X., Rollet, E., Clantin, B., Landrieu, I., Odberg-Ferragut, C., Lippens, G., Bohin, J. P., and Villeret, V. (2004) Structural analysis of *Escherichia coli* OpgG, a protein required for the biosynthesis of osmoregulated periplasmic glucans. *J. Mol. Biol.* **342,** 195–205
15. Kabsch, W. (2010) Integration, scaling, space-group assignment and post-refinement. *Acta Crystallogr. D Biol. Crystallogr.* **66,** 133–144
16. Vonrhein, C., Blanc, E., Roversi, P., and Bricogne, G. (2007) Automated structure solution with autoSHARP. *Methods Mol. Biol.* **364,** 215–230
17. Sheldrick, G. M. (2010) Experimental phasing with SHELXC/D/E. Combining chain tracing with density modification. *Acta Crystallogr. D Biol. Crystallogr.* **66,** 479–485
18. Langer, G., Cohen, S. X., Lamzin, V. S., and Perrakis, A. (2008) Automated macromolecular model building for x-ray crystallography using ARP/wARP version 7. *Nat. Protoc.* **3,** 1171–1179

19. Cowtan, K. (2006) The Buccaneer software for automated model building. 1. Tracing protein chains. *Acta Crystallogr. D Biol. Crystallogr.* **62,** 1002–1011
20. Zwart, P. H., Afonine, P. V., Grosse-Kunstleve, R. W., Hung, L. W., Ioerger, T. R., McCoy, A. J., McKee, E., Moriarty, N. W., Read, R. J., Sacchettini, J. C., Sauter, N. K., Storoni, L. C., Terwilliger, T. C., and Adams, P. D. (2008) Automated structure solution with the PHENIX suite. *Methods Mol. Biol.* **426,** 419–435
21. Emsley, P., Lohkamp, B., Scott, W. G., and Cowtan, K. (2010) Features and development of Coot. *Acta Crystallogr. D Biol. Crystallogr.* **66,** 486–501
22. Laskowski, R. A., MacArthur, M. W., Moss, D. S., and Thornton, J. M. (1993) PROCHECK. A program to check the stereochemical quality of protein structures. *J. Appl. Crystallogr.* **26,** 283–291
23. Holm, L., Kääriäinen, S., Rosenström, P., and Schenkel, A. (2008) Searching protein structure databases with DaliLite version 3. *Bioinformatics* **24,** 2780–2781
24. Kanamaru, S., Ishiwata, Y., Suzuki, T., Rossmann, M. G., and Arisaka, F. (2005) Control of bacteriophage T4 tail lysozyme activity during the infection process. *J. Mol. Biol.* **346,** 1013–1020
25. Weaver, L. H., Grütter, M. G., and Matthews, B. W. (1995) The refined structures of goose lysozyme and its complex with a bound trisaccharide show that the "goose-type" lysozymes lack a catalytic aspartate residue. *J. Mol. Biol.* **245,** 54–68
26. Vocadlo, D. J., Davies, G. J., Laine, R., and Withers, S. G. (2001) Catalysis by hen egg-white lysozyme proceeds via a covalent intermediate. *Nature* **412,** 835–838
27. Mende, J., and Braun, V. (1990) Import-defective colicin B derivatives mutated in the TonB box. *Mol. Microbiol.* **4,** 1523–1533
28. Mora, L., Diaz, N., Buckingham, R. H., and de Zamaroczy, M. (2005) Import of the transfer RNase colicin D requires site-specific interaction with the energy-transducing protein TonB. *J. Bacteriol.* **187,** 2693–2697
29. Zeth, K., Römer, C., Patzer, S. I., and Braun, V. (2008) Crystal structure of colicin M, a novel phosphatase specifically imported by *Escherichia coli*. *J. Biol. Chem.* **283,** 25324–25331
30. Hilsenbeck, J. L., Park, H., Chen, G., Youn, B., Postle, K., and Kang, C. (2004) Crystal structure of the cytotoxic bacterial protein colicin B at 2.5 Å resolution. *Mol. Microbiol.* **51,** 711–720
31. Matsumura, M., Becktel, W. J., Levitt, M., and Matthews, B. W. (1989) Stabilization of phage T4 lysozyme by engineered disulfide bonds. *Proc. Natl. Acad. Sci. U.S.A.* **86,** 6562–6566
32. Harkness, R. E., and Braun, V. (1990) Colicin M is only bactericidal when provided from outside the cell. *Mol. Gen. Genet.* **222,** 37–40
33. Guzman, L. M., Belin, D., Carson, M. J., and Beckwith, J. (1995) Tight regulation, modulation, and high level expression by vectors containing the arabinose PBAD promoter. *J. Bacteriol.* **177,** 4121–4130
34. Baase, W. A., Liu, L., Tronrud, D. E., and Matthews, B. W. (2010) Lessons from the lysozyme of phage T4. *Protein Sci.* **19,** 631–641
35. Kuroki, R., Weaver, L. H., and Matthews, B. W. (1993) A covalent enzyme-substrate intermediate with saccharide distortion in a mutant T4 lysozyme. *Science* **262,** 2030–2033
36. Saeidi, N., Wong, C. K., Lo, T. M., Nguyen, H. X., Ling, H., Leong, S. S., Poh, C. L., and Chang, M. W. (2011) Engineering microbes to sense and eradicate *Pseudomonas aeruginosa*, a human pathogen. *Mol. Syst. Biol.* **7,** 521
37. Arnold, T., Zeth, K., and Linke, D. (2009) Structure and function of colicin S4, a colicin with a duplicated receptor-binding domain. *J. Biol. Chem.* **284,** 6403–6413
38. Roos, U., Harkness, R. E., and Braun, V. (1989) Assembly of colicin genes from a few DNA fragments. Nucleotide sequence of colicin D. *Mol. Microbiol.* **3,** 891–902
39. Riley, M. A., and Wertz, J. E. (2002) Bacteriocin diversity. Ecological and evolutionary perspectives. *Biochimie* **84,** 357–364
40. Braun, V., Patzer, S. I., and Hantke, K. (2002) Ton-dependent colicins and microcins. Modular design and evolution. *Biochimie* **84,** 365–380
41. Ferber, D. M., and Brubaker, R. R. (1979) Mode of action of pesticin. *N*-Acetylglucosaminidase activity. *J. Bacteriol.* **139,** 495–501
42. Penfold, C. N., Healy, B., Housden, N. G., Boetzel, R., Vankemmelbeke, M., Moore, G. R., Kleanthous, C., and James, R. (2004) Flexibility in the receptor-binding domain of the enzymatic colicin E9 is required for toxicity against *Escherichia coli* cells. *J. Bacteriol.* **186,** 4520–4527
43. Duché, D., Baty, D., Chartier, M., and Letellier, L. (1994) Unfolding of colicin A during its translocation through the *Escherichia coli* envelope as demonstrated by disulfide bond engineering. *J. Biol. Chem.* **269,** 24820–24825
44. Zhang, Y., Vankemmelbeke, M. N., Holland, L. E., Walker, D. C., James, R., and Penfold, C. N. (2008) Investigating early events in receptor binding and translocation of colicin E9 using synchronized cell killing and proteolytic cleavage. *J. Bacteriol.* **190,** 4342–4350
45. Zakharov, S. D., Sharma, O., Zhalnina, M. V., and Cramer, W. A. (2008) Primary events in the colicin translocon. FRET analysis of colicin unfolding initiated by binding to BtuB and OmpF. *Biochemistry* **47,** 12802–12809
46. Duché, D. (2007) Colicin E2 is still in contact with its receptor and import machinery when its nuclease domain enters the cytoplasm. *J. Bacteriol.* **189,** 4217–4222
47. Chauleau, M., Mora, L., Serba, J., and de Zamaroczy, M. (2011) FtsH-dependent processing of RNase colicins D and E3 means that only the cytotoxic domains are imported into the cytoplasm. *J. Biol. Chem.* **286,** 29397–29407
48. Kleanthous, C. (2010) Swimming against the tide. Progress and challenges in our understanding of colicin translocation. *Nat. Rev. Microbiol.* **8,** 843–848
49. Anderson, W. F., Grütter, M. G., Remington, S. J., Weaver, L. H., and Matthews, B. W. (1981) Crystallographic determination of the mode of binding of oligosaccharides to T4 bacteriophage lysozyme. Implications for the mechanism of catalysis. *J. Mol. Biol.* **147,** 523–543
50. Tsugita, A. (1971) in *The Enzymes* (Boyer, P. D., ed) 3rd Ed., pp. 343–411, Academic Press, New York
51. Studier, F. W., and Moffatt, B. A. (1986) Use of bacteriophage T7 RNA polymerase to direct selective high level expression of cloned genes. *J. Mol. Biol.* **189,** 113–130
52. Miroux, B., and Walker, J. E. (1996) Overproduction of proteins in *Escherichia coli*. Mutant hosts that allow synthesis of some membrane proteins and globular proteins at high levels. *J. Mol. Biol.* **260,** 289–298
53. Rakin, A., Saken, E., Harmsen, D., and Heesemann, J. (1994) The pesticin receptor of *Yersinia enterocolitica*. A novel virulence factor with dual function. *Mol. Microbiol.* **13,** 253–263